

University of Stuttgart
Institute of Industrial Automation and
Software Engineering

This thesis is
confidential.

Quality-Based Path Planning

Algorithm Development for Automated 3D Inspection Using 3D Scanners

Research project No.3647

Submitted at the University of Stuttgart by
Xu Wang

Forschungsarbeit

Examiner: Prof. Dr.-Ing. Michael Weyrich
Supervisor: Prof. Dr.-Ing. Nasser Jazdi
External Supervisor: Dr.-Ing. Kun Zhan (Shining3d
Technology GMBH)

01.07.2024



Table of Contents

TABLE OF CONTENTS	II
TABLE OF FIGURES	IV
TABLE OF TABLES	VI
ABSTRACT	VII
1 INTRODUCTION	8
1.1 Background	8
1.2 Research Objectives and Goals	9
1.3 Thesis Structure Overview	10
2 LITERATURE REVIEW	12
2.1 The View Planning Problem	12
2.2 Approaches based on a priori knowledge	13
2.3 Sumamry	15
3 MODEL-BASED VIEWPOINTS GENERATION METHOD	16
3.1 Candidate Viewpoint Generation Strategy	16
3.1.1 Analysis of the Measurable Area of the 3D Scanner	17
3.1.2 Measurement Space Estimation and Verification	24
3.1.3 Candidate Viewpoint Generation	26
3.2 Optimal Viewpoint Selection Strategy	29
3.2.1 Determining Measurement Constraints of the Scanner	29
3.2.2 Optimal Viewpoint Selection	34
3.3 Determination of Key Algorithm Parameters	37
4 COMPLEX SURFACE MODEL MEASUREMENT EXPERIMENT	41
4.1 Experimental Setup	41
4.1.1 Design of the Automated 3D Reconstruction System	41
4.1.2 Calibration of the Automated 3D Reconstruction System	43
4.2 Analysis of Scanning Results	50
4.2.1 Comparison of Single Frame Point Clouds	50
4.2.2 Analysis of Model Scanning Results	53
5 SUMMARY AND OUTLOOK	59
5.1 Summary	59
5.2 Limitations and Future Work	60

BIBLIOGRAPHY	63
DECLARATION OF COMPLIANCE	66

Table of Figures

Figure3-1 : The principle of the 3D structured light scanning system	16
Figure3-2: FOV region	18
Figure 3-4: FOV range of single and binocular cameras	19
Figure 3-4: DOF range of single camera	19
Figure 3-5: DOF range of single camera	20
Figure 3-6: DOF Intersection of binocular cameras	21
Figure 3-7: DOF Intersection of a binocular stereo vision system	23
Figure 3-8: The simplification procedure of effective measurement range.	24
Figure 3-9: Block unit division for big object	26
Figure 3-10: Candidate viewpoints set	28
Figure 3-11: The pose of the scanner	29
Figure 3-12: The visibility constraint of a single camera	30
Figure 3-13: The visibility constraint for a binocular structured light scanner	31
Figure 3-14: Occlusion Constraint Determination	32
Figure 3-15: Procedure of Optimal Viewpoint Selection	36
Figure 3-16: Relationship between the number of viewpoints and scanning coverage under different weight coefficient.....	38
Figure 3-17: The quality distribution of surface patches under different weight coefficients	39
Figure 4-1: Setup of automated measurement system	41
Figure 4-2: The calibration of the 3D Scanner	46
Figure 4-3: Validation of the ray casting effect in simulation environment	48
Figure 4-4: The calibration of the system in RobotDK	49
Figure 4-5: Ray casting result in simulation environment from zenith viewpoint	51
Figure 4-6: Point cloud results from zenith viewpoint in the experimental environment under different projector brightness	52

Figure 4-7: The comparison tof actual scanning point cloud and the ray casting simulation results	55
Figure 4-7: The point cloud result of the test sample	56
Figure 4-8: The comparison tof actual scanning point cloud and the ray casting simulation results	57
Figure 4-9: The point cloud result of the test sample	57

Table of Tables

Table 3.1: Candidate Viewpoint Generation	27
Table 4.1: Parameters of Robot Arm	42
Table 4.2: Parameters of of Turntable	43
Table 4.3: Parameters of of Structured Light Scanner	43
Table 4.4: Calibration information of left camera	46
Table 4.5: Calibration information of right camera	47

Abstract

Structured light 3D measurement technology is a non-contact optical method known for its high precision, speed, and resolution. It is widely used in industrial inspection, reverse engineering, and biomedical fields. However, traditional systems require manual operation, limiting their ability to meet high-speed, large-scale inspection demands. Combining structured light 3D measurement with industrial robots for automation is a key trend in developing high-performance 3D sensors for future digital factories.

The main challenge in automating structured light 3D measurement is the planning of measurement viewpoints and paths. Currently, this process relies on experienced engineers for manual teaching, which is time-consuming, dependent on expertise, and often suboptimal, leading to low efficiency.

To address these issues, this thesis explores techniques for generating measurement viewpoints and planning paths in automated structured light 3D measurement. A Generate & Test model-based method for automatic viewpoint generation is proposed. This method establishes an ellipsoidal measurement space constraint based on model characteristics and generates candidate viewpoints. It then determines the effective measurement range and optimal viewpoint criteria based on the scanner's design parameters. Using optical visibility, image quality, and surface coverage as constraints, a viewpoint quality evaluation function iteratively filters the candidate viewpoints, generating a set of high-quality measurement viewpoints.

Building on the viewpoint generation technique, this thesis further investigates path planning from these viewpoints and validates the scanning process in practical environments. A path planning method and experimental setup for automated structured light 3D measurement are proposed.

Based on these methods, a structured light automated 3D measurement planning system was developed on Shining3d's RobotScan platform. This system automatically generates measurement viewpoints and plans paths from 3D model files, and it has been practically applied to the automated measurement of complex curved parts. Experiments show that this planning system is fast and efficient, capable of replacing manual teaching in actual operations.

Key Words: Structured Light 3D Measurement, Automated Measurement, Viewpoint Generation, Path Planning, Industrial Robots, 3D Scanning

1 Introduction

1.1 Background

In many industrial applications, the reconstruction of high-resolution 3D virtual models has become mainstream. The ability to reverse engineer and specifically reconstruct or update 3D models of machined parts, buildings, historical monuments, landforms, and human bodies holds considerable significance in the context of Industry 4.0, building information modeling (BIM), and cultural heritage applications. With the emergence of increasingly accurate and convenient acquisition methods such as optical sensors, robot arms, and drones, the demand for 3D reconstruction has significantly increased across various domains, particularly in manufacturing control.

In the realm of product dimension measurement, 3D measurement devices based on structured light technology have gained widespread adoption due to their non-contact nature, high precision, fast speed, and high resolution. However, traditional structured light 3D measurement equipment requires manual operation, involving human intervention in communication, process control, and equipment positioning, making it challenging to meet the demands of intelligent manufacturing. The integration of structured light 3D measurement devices with industrial robots to achieve automated 3D measurement represents a trend in the development of high-performance 3D sensors for future digital factories.

The focal point and challenge of automated structured light 3D measurement lie in the planning of measurement viewpoints and paths. Automated measurement involves positioning a structured light 3D scanner by a multi-degree-of-freedom robot to move along a planned path and measure objects from multiple viewpoints to obtain complete 3D data. During the measurement process, viewpoints directly influence the measurement posture and data quality of the 3D scanner, while the measurement path determines the feasibility and efficiency of the measurement task. Currently, reliance on experienced engineers for manual teaching to edit measurement viewpoints and plan paths is time-consuming and often fails to achieve the optimal measurement viewpoints and paths, resulting in increased measurement time and limiting the efficiency of automated measurement devices.

To address these challenges, many research institutions have begun investigating techniques for automatic measurement viewpoint and path planning. This technology analyzes and quantifies the relationship between workpieces, measurement devices, and measurement task requirements, formulating constraints to automatically filter or create optimal viewpoints and plan measurement paths. Automated planning of measurement viewpoints and paths improves measurement efficiency and maximally satisfies the requirements of intelligent manufacturing.

1.2 Research Objectives and Goals

This thesis aims to develop a novel planning algorithm to improve the outcomes of the Visual Coverage Planning Problem (VCPP) and apply it to scenarios involving 3D scanning, shape reconstruction, and inspection using industrial robotic arms. The main research objectives and goals are outlined as follows.

Traditional robotic path planning problems typically focus on factors such as scan coverage, discrete viewpoints, collision avoidance, and speed to determine the optimal path. However, this study emphasizes the evaluation of scan quality in the context of 3D inspection. By leveraging pre-existing CAD models and geometric dimensioning and tolerancing (GD&T) information, an ellipsoidal measurement space constraint is established, and a set of candidate viewpoints is generated. Considering the parameters of the structured light scanner (such as projector size, camera sensor information, field of view, depth of field, the spatial relationship between the projector and the camera, and the design of the scanner's data acquisition algorithm), a simulation environment for scanning is constructed.

In this simulation environment, an objective function for viewpoint quality evaluation is created using constraints such as optical visibility, scan quality, and surface coverage. Through continuous testing, the optimal weight combination for this objective function is determined. Subsequently, the candidate viewpoints are iteratively filtered using the generated simulation environment and objective function, resulting in a set of high-quality measurement viewpoints.

Building on the viewpoint generation technique, this thesis further explores path planning from these viewpoints and designs an efficient and flexible measurement strategy. An automated 3D measurement system combining a structured light scanner, a robotic arm, and a rotating platform is developed. The system is first calibrated, and then the automated 3D scanning experiments are conducted on test objects. The scanning process is validated in practical environments.

Ultimately, this method provides high-quality point cloud data for 3D inspection. The key advantage of this approach is that it not only considers traditional path planning factors but also prioritizes scan quality as the main evaluation criterion, thereby meeting the specific requirements of the application scenario.

In the current research landscape, common viewpoint planning and path planning methods tend to focus solely on surface coverage and scanning efficiency. However, in the practical application of 3D inspection, it is imperative not only to consider the coverage of data but also to ensure the high-precision alignment of scanning data with reference data. This process involves meticulous comparative inspection of both global and local geometric features. The quality of scanning data directly affects the accuracy of geometric construction, which is influenced by a variety of factors, including the distance between the scanner and the object, the normal angle of the object's surface, as well as differences in brightness and surface material. Precise

quantitative analysis of these parameters that affect scanning quality is crucial for enhancing the effectiveness of viewpoint and path planning.

Although existing studies have made certain progress in simulation calculations, most have not delved into the translation of simulation results into real-world scanning data. This paper fills this gap by comparing simulated calculations with real-world scanning data, verifying the validity of virtual scanning data, and revealing the differences between it and actual scanning data. This discovery not only confirms the potential of simulation in predicting real scanning effects but also provides valuable insights on how to utilize 3D scanners to obtain higher quality data in real-world applications.

1.3 Thesis Structure Overview

This thesis combines the current state of research in structured light automated 3D measurement technology with viewpoint and path planning techniques. It delves into viewpoint generation and automated 3D measurement technologies, proposing a method for automatic viewpoint generation as well as path planning and testing methods specifically tailored for structured light automated measurement. Based on this, an automated measurement planning system and an automated 3D measurement platform are developed. The organization of this thesis is as follows:

- **Chapter 1** introduces the background and significance of viewpoint and path planning techniques in structured light automated 3D measurement. It also briefly outlines the research objectives and goals.
- **Chapter 2** provides a comprehensive literature review on solving the View Planning Problem (VPP) in 3D reconstruction. The review highlights key methods for generating viewpoints, and discusses various objective function criteria used in VPP, such as surface coverage, scan direction optimization, occlusion effects, scan overlap, avoiding collisions, and scanning time optimization.
- **Chapter 3** focuses on the existing measurement viewpoint planning technologies and investigates the automatic generation of viewpoints. It proposes a method for automatic viewpoint generation, introduces the relevant theories, and explains the imaging constraints of 3D sensors. Through the establishment of a mathematical model, the chapter elucidates the process and principles of the proposed viewpoint generation algorithm.
- **Chapter 4** designs an efficient and flexible measurement strategy and constructs an automated 3D measurement system that integrates a structured light scanner, a robotic arm, and a rotating platform. The system is first calibrated, followed by the execution of automated 3D scanning experiments on test objects. The

effectiveness of the viewpoint generation algorithm is validated by comparing and discussing the simulation and actual scanning data.

- **Chapter 5** summarizes the completed work and provides an outlook on future research directions.

2 Literature Review

With the advancement of optical sensors, robotic arms, drones, and other technologies, 3D reconstruction has become increasingly precise and convenient. Consequently, the practicality of 3D reconstruction has grown significantly in fields such as manufacturing control and building surveillance, leading to a substantial increase in demand.

In recent years, the accuracy of laser scanners and structured light projection devices has improved significantly, meeting the needs of automated quality control and reverse engineering in industrial production. However, in the industrial sector, quality inspections of products are typically conducted at specific times and locations, making it challenging to integrate them into the production line and synchronize them with the production pace. This configuration increases cycle time and the final cost of parts.

In 2018, Zhang [1] presented a comprehensive review of the latest advancements in various measurement methods based on structured light, discussing the advantages and disadvantages of this technology . One of the critical steps in promoting the automatic reconstruction of 3D objects is viewpoint planning, known as the Viewpoint Planning Problem (VPP). VPP aims to automatically determine the optimal positions and/or trajectories for the acquisition method to achieve complete coverage of the considered part. In 2021, Manon [2] similarly introduced and summarized the latest developments in full-process technology, various measurement methods, and evaluation standards based on structured light.

2.1 The View Planning Problem

The View Planning Problem (VPP) can be approached in two distinct ways: with or without prior knowledge of the object to be digitized. Methods that utilize prior knowledge generally employ a CAD model or a mesh as the input. In contrast, methods that do not use such knowledge start from an initial position and determine subsequent positions in real time.

The objective of solving the VPP is to determine the minimum number of views required to reconstruct the object in 3D. A common approach is to generalize the VPP as a set covering problem (SCP). The SCP involves finding the smallest number of subsets whose union covers the entire set. In the context of VPP, this means identifying the fewest number of scans that cover all necessary parts of the object's surface.

In 2001, Scott [3] et al. introduced a method to convert the VPP into the SCP. By dividing the outer surface of a 3D object into multiple patches and having each scan overlap with a set of these patches, the objective is to maximize the coverage with the fewest number of scans. The SCP is a well-known optimization problem, and in 1972, Karp [4] demonstrated that the SCP, among 21 other problems, is NP-complete. This implies that no polynomial-time solution exists for this problem.

2.2 Approaches based on a priori knowledge

To address the View Planning Problem, the first step involves processing the object's surface to make it suitable for analysis. Among the various surface segmentation methods, the most common approach is to use a mesh of the object and consider each face of the mesh as a patch. This approach can handle different levels of detail, often using a simplified mesh to approximate the object's shape. Researchers like Loriot [5], Scott et al. [6], and Mahmud et al.[7] have employed this method because it reduces algorithm complexity and calculation time. However, this approach may lose surface self-occlusions in complex objects. Jing et al. [8] utilized the bubble mesh algorithm, which generates a uniform triangular mesh while preserving the original shape, resulting in patches of similar size. Another segmentation method involves positioning the object in a grid of voxels.

Another crucial aspect of addressing the View Planning Problem (VPP) is the generation of candidate viewpoints. If the generated viewpoints do not adequately cover the surface, the VPP cannot be effectively solved. These methods can be broadly categorized into analytical generation methods and spatial sampling methods.

Analytical Generation Methods:

- Orientation with Surface Normals: A common method involves generating viewpoints aligned with the surface normals of each patch. This approach, used by researchers like Scott[9], Martins[10], and Mahmud[7], is straightforward but heavily depends on surface segmentation. Coarse segmentation may result in the loss of important features due to inadequate consideration of self-occlusions.
- Point Normals: Scott et al.[11] and Loriot[12] generated viewpoints along the normals to each surface point. This method also applies filters to reduce complexity but remains dependent on the segmentation step.

Spatial Sampling Methods:

- Random Sampling in Volume Space: Jing[13,14] et al. used random sampling within a volume defined by the camera's minimum and maximum field distances. Viewpoint orientations were computed based on an attraction force model. This

method can result in missed surface areas due to the randomness of viewpoint positions.

- Sampling in Robot Kinematic Space: Jing et al.[15] sampled viewpoints on an ellipsoidal hemisphere and defined a robot configuration for each viewpoint. Viewpoints causing collisions or inaccessible to the robot were discarded. This method is constrained by the robot's workspace.
- Iterative Random Sampling: Mohammadikaji et al.[16] used iterative random sampling, renewing viewpoints in each iteration based on the sensor and model support. This increases the chances of finding optimal viewpoints but is computationally intensive.

Also, when addressing the View Planning Problem (VPP), it is essential to establish an objective function to determine the optimal viewpoints. However, the methods and focus for defining these objective functions can vary. Here are some common criteria for objective functions:

- **Surface Coverage:** A common method for solving the SCP is to maximize surface coverage while minimizing the number of viewpoints. These algorithms achieve this by minimizing or maximizing a cost function or objective function, the definition of which is crucial to the result. Surface coverage is the first criterion. Researchers such as Scott [6,9,11], Loriot[12], Krause[16], Jing[8], Hepp[18], Fan[20], Martins[10], and Ren[19] have integrated this criterion into their objective functions. Mohammadikaji, for instance, focused on covering specific regions of the CAD model rather than achieving complete coverage at all costs.
- **Scan Direction Optimization:** In addition to optimizing surface coverage, Jing[8], Hepp[18], Martins[10], Fan[20] and Ren[19] have attempted to optimize the scanner's direction based on the surface normal. This approach helps enhance the quality of the point cloud.
- **Occlusion Effects:** To evaluate the surface coverage from a viewpoint, Jing [8] and Hepp[10] considered the effects of occlusions. Methods by Loriot [12] simplify the model to attempt to scan only the simplified version. Depending on the simplification rate, certain parts of the real surface may not be reached due to unconsidered occlusions.
- **Scan Overlap:** Another key criterion is the overlap between scans. In computer graphics, registration algorithms rely on identifying common parts between two point clouds to align them. When planning a complete scan, multiple alignments are needed to reconstruct the entire part's point cloud. Therefore, it is crucial to optimize each viewpoint in the scan plan to ensure it has at least one part in common with another viewpoint. Researchers such as Scott[], Krause[16], Fan[20] have used this criterion in their objective functions.

- **Avoiding Collisions:** During scanning, collisions between the acquisition devices, the object to be scanned, and environmental obstacles should be avoided. Researchers like Scott [6,9,11], Hepp[18] and Martins have integrated collision criteria directly into their objective functions to avoid selecting viewpoints that would result in collisions with surrounding elements.
- **Scanning Time Optimization:** In industrial applications, scan plans are used to inspect and control parts to reduce inspection time. Hepp[18] and Jing[8] included a criterion to optimize inspection time in their objective functions. This involves considering the distance between a newly identified viewpoint and previously selected viewpoints. The type of distance can vary depending on the sensor's mode of movement (e.g., robot or drone).

2.3 Sumamry

In this chapter, we discussed the relevant work on solving the View Planning Problem (VPP) in 3D reconstruction. We examined two primary approaches: those utilizing prior knowledge of the object and real-time methods. Key methods for generating viewpoints include analytical generation and spatial sampling techniques. The review highlighted various objective function criteria used in VPP, such as surface coverage, scan direction optimization, occlusion effects, scan overlap, avoiding collisions, and scanning time optimization. A brief overview of corresponding algorithms and their applications in industrial and research contexts was also described.

3 Model-Based Viewpoints Generation Method

This chapter details the generation of candidate viewpoints and the selection of optimal viewpoints during 3D reconstruction. It involves the analysis of the measurable area of the 3D measurement system through the establishment of a mathematical model and proposes a candidate viewpoint set generation strategy based on the known model. Subsequently, a simulation environment and an optimal viewpoint selection strategy are established based on the scanner's design information and optical parameter constraints.

3.1 Candidate Viewpoint Generation Strategy

The principle of the 3D structured light scanning system is illustrated in Figure3-1. This system encodes phases into the structured light in the form of stripes. When the projector casts these sinusoidal fringe patterns onto the surface of the object, the height variations of the object's surface modulate the patterns. The camera captures the deformed fringe images, which are then decoded to calculate the phase values of the pixels within the field of view. Through epipolar constraint matching of the left and right camera images, binocular stereo vision is used to derive the 3D coordinates of points on the object's surface, thereby achieving 3D reconstruction of the object. The point cloud data obtained from structured light scanning are characterized by high density and accuracy, making it suitable for the 3D scanning and reconstruction of complex-shaped objects.

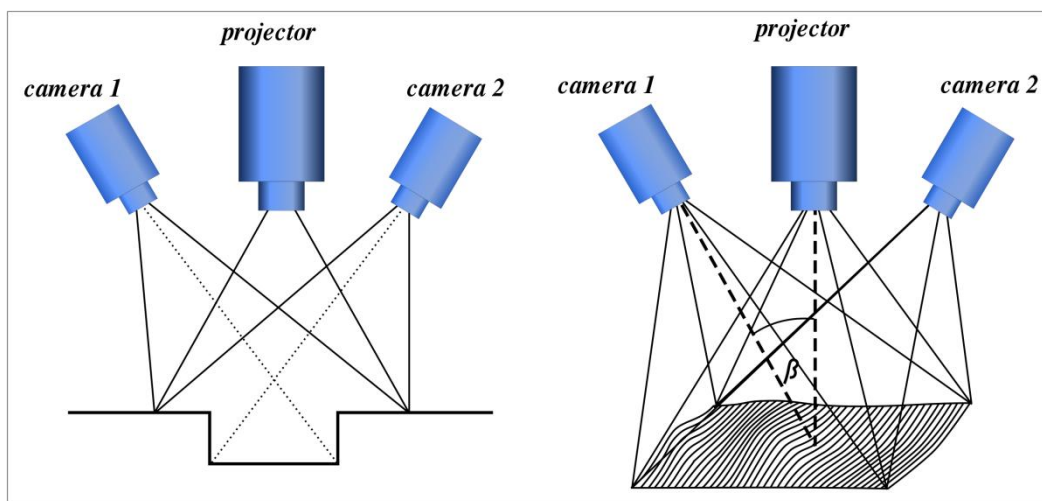


Figure3-1 : The principle of the 3D structured light scanning system. (Wikipedia contributors. (n.d.). 3-proj2cam.svg [SVG file]. Wikimedia Commons. <https://commons.wikimedia.org/wiki/File:3-proj2cam.svg>)

A typical method for viewpoint planning is the block division method. In viewpoint planning, block units are established based on the scanner's field of view and depth of field. The model is divided into multiple regions using these block units, with viewpoint generation tasks conducted separately within each region. A candidate viewpoint is generated at the optimal measurement distance on each unobstructed grid surface for further selection. This method simplifies the process of feature extraction and analysis, thereby reducing the difficulty of viewpoint generation.

However, the depth of field range of a binocular structured light scanner is large, and the grid size is larger than that generated by traditional methods. Additionally, a single viewpoint on each block surface cannot ensure the effective scanning of the model within that region. Therefore, this thesis improves the grid-based viewpoint planning method to better suit the characteristics of binocular structured light reconstruction.

Based on the analysis of the measurable area of the 3D scanner, the grid unit size is determined. Candidate viewpoints are generated using an adaptive scheme that takes into account the grid unit size and the optical constraints of the 3D scanner, achieving higher utilization of the measurable area. This scheme can adaptively handle objects of various sizes. For large objects, the block division method is used to create multiple block units, with each block unit generating a corresponding set of candidate viewpoints. For objects with a bounding box smaller than the size of a block unit, candidate viewpoints are generated based on the characteristics of the bounding box.

3.1.1 Analysis of the Measurable Area of the 3D Scanner

Before the binocular structured light scanner can perform scanning and reconstruction, camera calibration and projector calibration are required. Once calibration is complete, the focal length, aperture value, and focusing distance of the camera and projector are fixed, establishing the optical parameter constraints of the scanner. By combining the spatial position and angle between the camera and projector with the design information, the effective measurement range of the binocular structured light scanner can be determined.

The optical parameter constraints mainly include depth of field and field of view, while the design information primarily involves the distance and angle between the camera and the projector. With this information, the effective measurement range of the binocular scanner can be calculated. The block unit is then derived by simplifying this measurement range.

3.1.1.1 Field of View Constraints

The field of view (FOV) of a camera is limited by the sensor size and lens focal length. Whether using an optical camera or a digital camera, only images within a certain angle can be captured, as this angle determines the range of light projected onto the photosensitive element. Surface points beyond the sensor area will be projected outside the sensor region. Generally, the FOV region is a quadrangular pyramid. As shown in Figure 3-2, the lens center along the optical axis direction is the visual sensor's line of sight. To ensure that the object is always within the FOV during each capture, the object must remain within the spatial range of the view cone.

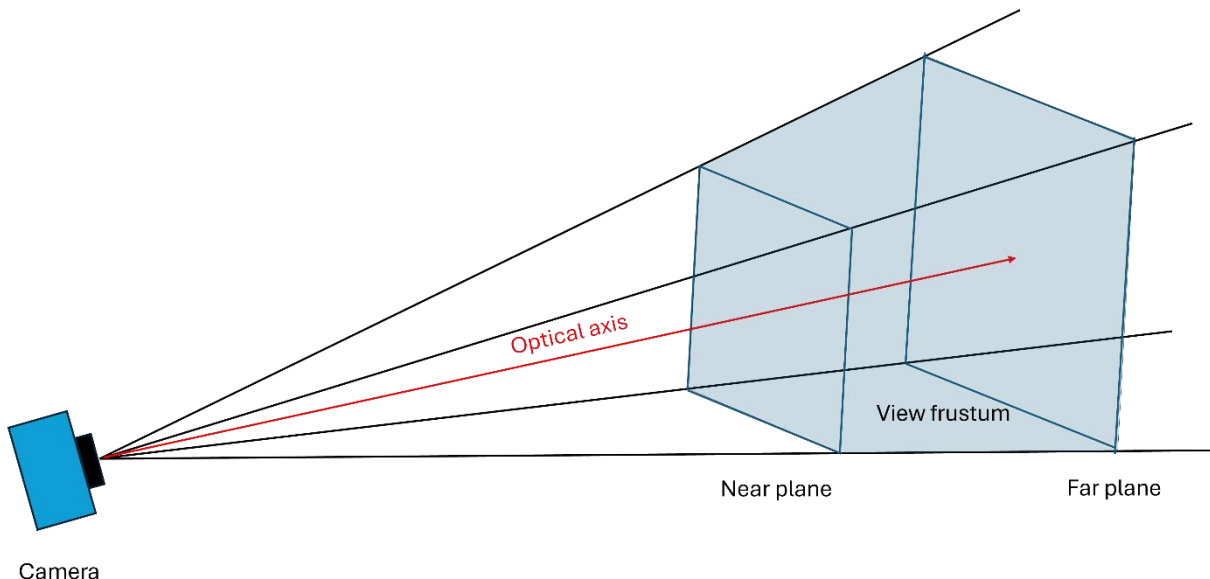


Figure3-2: FOV region

Based on the shape of the optical sensor and the design of the camera optical system, it is generally assumed that the image plane is symmetrical about the optical axis. The FOV constraints are as follows:

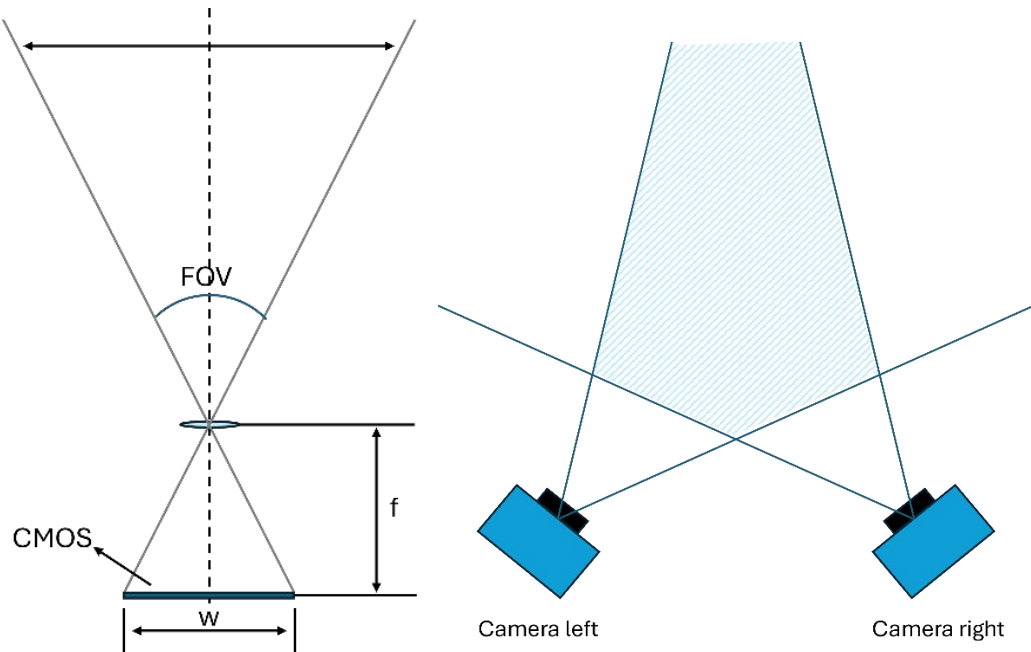
$$FOV_{Horizontal} = 2 * \tan^{-1} \frac{w}{2f}$$

$$FOV_{Vertical} = 2 * \tan^{-1} \frac{h}{2f}$$

$$FOV_{Diagonal} = 2 * \tan^{-1} \frac{d}{2f}$$

Where, w is the width of the CMOS sensor, h is the height of the CMOS sensor, and d is the diagonal length of the CMOS sensor.

For a binocular stereo vision system, it is necessary to consider the overlap of the binocular FOVs. For structured light vision sensors, both the camera and the optical sensor need to be considered. The FOV range of single and binocular cameras is illustrated in Figure 3-4.



(a) FOV range of single camera (b) FOV range of binocular cameras

Figure 3-4: FOV range of single and binocular cameras

3.1.1.2 Depth of Field Constraints

The depth of field (DOF) is the distance between the nearest and the farthest objects in an image that appear acceptably sharp. When capturing images, the camera is focused on objects at various distances. The distance to the nearest point in acceptably sharp focus in front of the best-focused point is called the front depth of field, whereas the distance to the farthest point in acceptably sharp focus behind the best-focused point is called the rear depth of field. The total distance between these points is the depth of field.

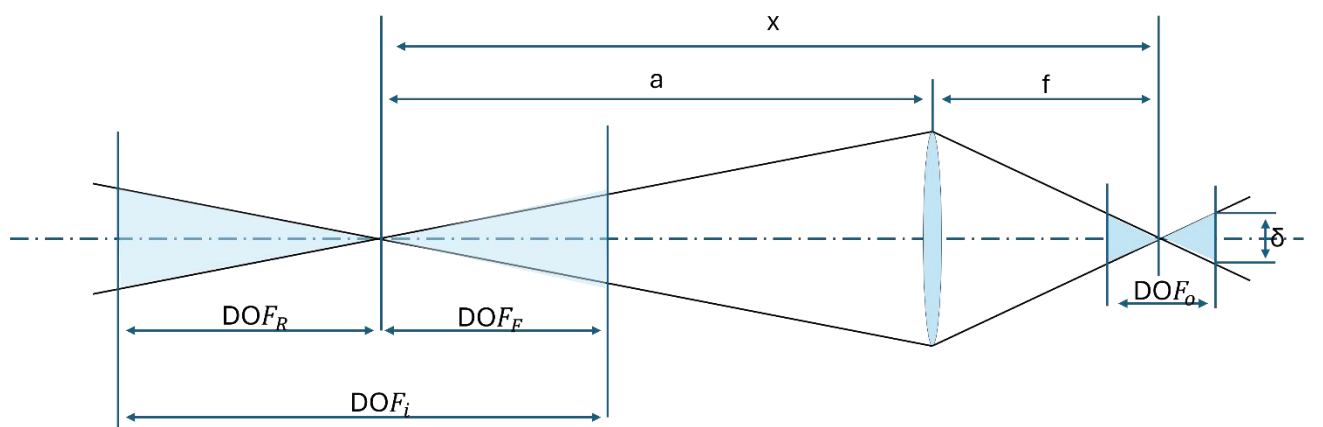


Figure 3-4: DOF range of single camera

The camera's DOF is closely related to its focal length (f), focus distance (D), aperture value (F), and other parameters, as illustrated in **Figure 3-4**. Once the industrial camera on the structured light scanner is calibrated, its aperture, focal length, and focus distance are known. Based on these system parameters, the DOF can be calculated using the following formula:

$$DOF_i = DOF_F + DOF_R$$

$$DOF_F = \frac{\delta * F_e * x^2}{f^2 - \delta * F_e * x}$$

$$DOF_R = \frac{\delta * F_e * x^2}{f^2 + \delta * F_e * x}$$

Where:

- DOF_o is the depth of focus,
- DOF_i is the depth of field (absolute value),
- DOF_F is the front depth of field,
- DOF_R is the rear depth of field,
- f is the focal length,
- F_e is the effective f-number,
- δ is the diameter of the Airy disk(abbreviated as CoC),
- a is the subject distance(from the front principal point).

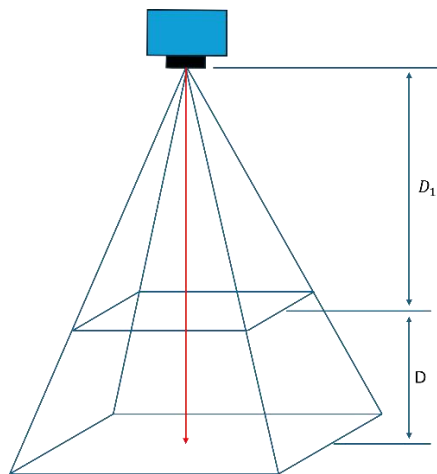


Figure 3-5: DOF range of single camera

For a binocular stereo vision system, the overlap of the fields of view of both cameras needs to be considered. Figure 3-5 illustrates the effective measurement range for

single and binocular cameras. In Figure 3-5 the effective measurement range of a single camera is depicted, where D_1 represents the near depth of field, D represents the depth of field range, and H is the optimal measurement distance for a single camera. Figure 3-6 shows the front view of the effective measurement range for binocular cameras. In this figure, Region 1 indicates the effective measurement range of the binocular cameras. The distance between the two cameras is L , with Camera 1 as the reference camera. In the front view, the field of view angle is θ . The boundaries of the field of view for Camera 1 are l_1 and l_2 , while the boundaries for Camera 2 are l_3 and l_4 . The near depth of field boundaries for both Camera 1 and Camera 2 are l_5 and l_6 .

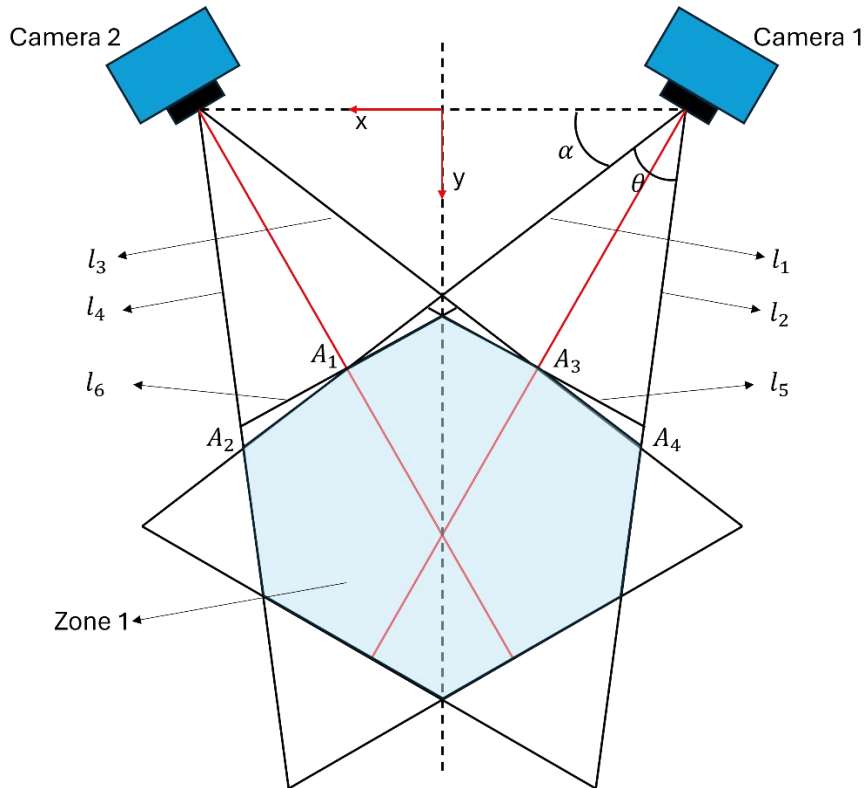


Figure 3-6: DOF Intersection of binocular cameras

In Figure 3-6, a planar coordinate system is established with the centers of the two cameras as the origin. The direction from Camera 1 towards Camera 2 is defined as the X-axis, and the direction from the origin towards the object to be measured is defined as the Y-axis. The angle between the upper boundary of Camera 1's field of view and the X-axis is denoted as α . Therefore, the equations of the boundary lines for the fields of view and depth of field of the two cameras can be expressed as follows:

$$l_1 = \tan \alpha * (x + \frac{L}{2})$$

$$l_2 = \tan(\alpha + \theta) * (x + \frac{L}{2})$$

$$l_3 = -\tan \alpha * (x - \frac{L}{2})$$

$$l_4 = -\tan(\alpha + \theta) * (x - \frac{L}{2})$$

$$l_5 = -\tan \varepsilon_1 * \left(x + \frac{L}{2} - D_1 \cos \varepsilon_2 \right) + D_1 \sin \varepsilon_2$$

$$l_6 = \tan \varepsilon_1 * \left(x - \frac{L}{2} + D_1 \cos \varepsilon_2 \right) + D_1 \sin \varepsilon_2$$

Where,

$$\varepsilon_1 = 90 - \alpha - \frac{\theta}{2}$$

$$\varepsilon_2 = \alpha + \frac{\theta}{2}$$

By referring to Figure 3-6, the intersection points can be determined as follows:

- Intersection point $A_1(x_1, y_1)$ is where l_1 intersects l_6 .
- Intersection point $A_2(x_2, y_2)$ is where l_1 intersects l_4 .
- Intersection point $A_3(x_3, y_3)$ is where l_3 intersects l_5 .
- Intersection point $A_4(x_4, y_4)$ is where l_3 intersects l_2 .

3.1.1.3 Projector Constraints

In a binocular stereo vision system based on structured light, a digital light processing (DLP) projector is used to project sinusoidal fringes. Generally, projectors have a larger field of view but a smaller depth of field, which makes the effective measurement range of the binocular scanner smaller than that of the binocular cameras alone. Figure 3- 7 illustrates the effective measurement range of the binocular scanner, with Zone 2 representing the effective measurement range of the binocular scanner.

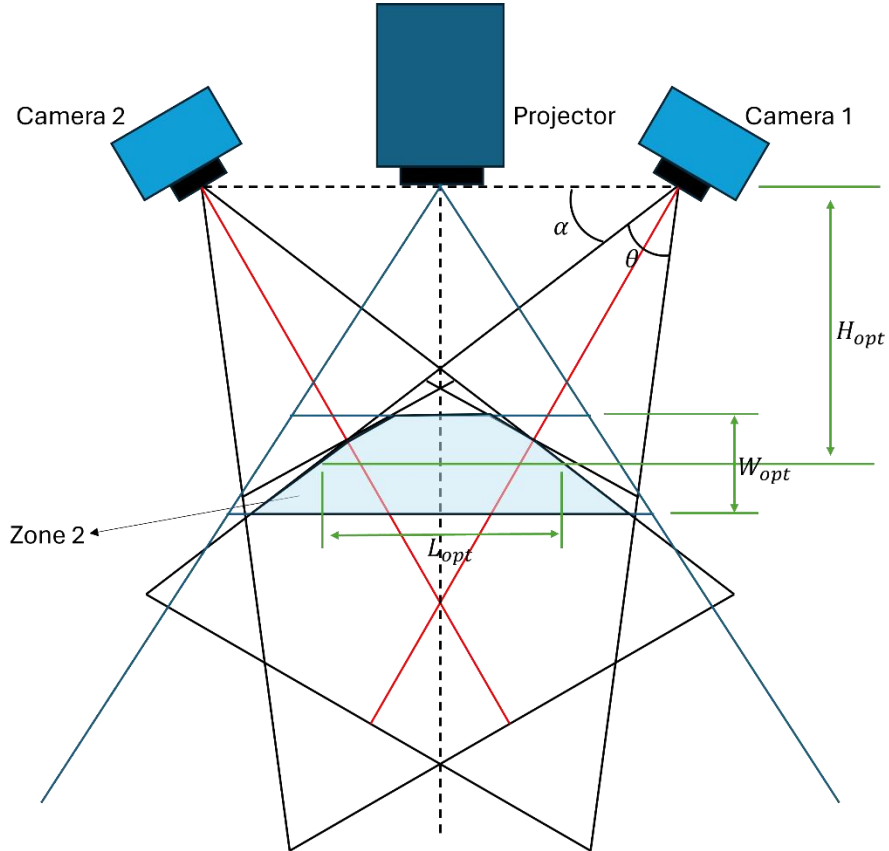


Figure 3-7: DOF Intersection of a binocular stereo vision system

Figure 3-7 illustrates the simplified scanning cone and grid units within Region 2. For the scanning cone, the direction of the Z-axis is determined based on the right-hand rule, and this coordinate system is used to describe the scanner's pose. The main parameters of the scanning cone and grid units are defined as follows:

$$W_{opt} = \frac{(y_2 - y_1) + (y_4 - y_3)}{2}$$

$$L_{opt} = \frac{(x_1 - x_3) + (x_2 - x_4)}{2}$$

$$H_{opt} = y_1 + \frac{(y_2 - y_1) + (y_4 - y_3)}{2}$$

In these equations, H represents the optimal measurement distance of the binocular scanner, W is the height of the scanning frustum, and L is the width of the frustum at the optimal plane.

By further simplifying this scanning frustum, it can be represented as a rectangular cuboid with a length of L_{opt1} , a width of L_{opt2} , and a height of W_{opt} . This rectangular cuboid can be used as a reference to determine the size of the block units in the block division method. The simplification procedure is showed as Figure 3-8.

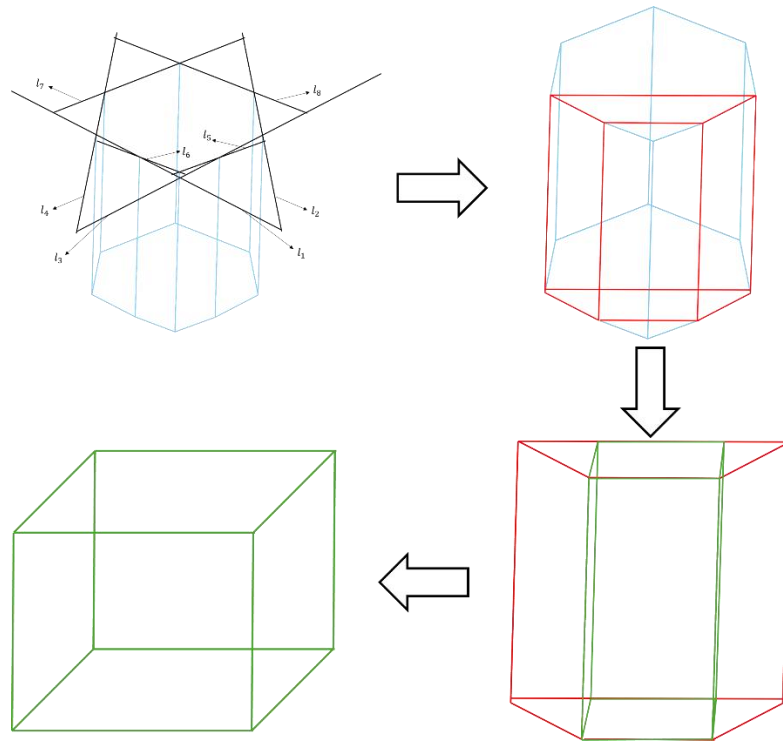


Figure 3-8: The simplification procedure of effective measurement range.

3.1.2 Measurement Space Estimation and Verification

In this study, we use the TranscanC 3D structured light scanner from Shining 3D GMBH. This is a professional-grade white light high-precision 3D scanner capable of capturing ultra-high resolution and accurate scans of small to medium-sized objects for various industries. It achieves an accuracy of up to 0.035 mm, which meets the requirements of this experiment. The binocular system consists of two SVD industrial cameras and a high-resolution projector, as shown in Figure 3-9.



Figure 3-9: TranscanC 3D structured light scanner

Before performing scanning and reconstruction, the binocular structured light scanner requires camera calibration and projector calibration. After calibration, the focal length, aperture value, and focus distance of the cameras and projector are fixed. These parameters can be obtained by decoding the calibration files. At this point, the optical parameter constraints of the two industrial cameras are determined. Combining these with the camera sensor parameters and projector parameters, the effective measurement range of the binocular structured light scanner is established.

This scanner utilizes Hikvision's MV-CE120-10UM/UC economical area scan cameras, equipped with CMOS sensors that offer low noise and high resolution of 4000×3036 (12.14 million pixels). The pixel size is $1.85 \mu\text{m} \times 1.85 \mu\text{m}$, providing excellent image quality, and the maximum frame rate at full resolution reaches up to 31.9 fps. The distance between the two cameras is 202 mm, with an included angle of 23° . By combining the field of view (FOV) and depth of field (DOF) information obtained through calibration, the initial size of the camera's view cone can be calculated.

The projector, after calibration, has a depth of field of approximately 480 ± 100 mm and a projection area of 300×190 mm on the optimal focus plane. With this information, we can estimate the measurement space size by establishing a mathematical model. By substituting the parameters from the calibrated 3D sensor into the above equations, we can theoretically simplify the measurement space to a rectangular cuboid with its center 480 mm in front of the viewpoint along the optical axis, and dimensions of $275 \times 175 \times 80$ mm.

Next, the actual measurement space is determined through practical measurement and compared with the theoretical values. It was found that the imaging mode of the 3D scanner differs from that of a conventional digital camera, and its working depth of field cannot be directly calculated using standard optical depth of field formulas. Specifically, the actual working depth of field and depth of focus of the 3D scanner are larger than those of a typical optical system. Even when the imaging point on the sensor is slightly larger than the optical circle of confusion, the scanner can still generate point cloud data through algorithmic optimization. The actual working depth of field, measured practically, ranges from approximately 480-70 mm to 480+85 mm.

By combining practical tests and estimates, we adjust the theoretical measurement space to obtain an actual measurement space of a rectangular cuboid with its center 480 mm in front of the viewpoint along the optical axis, and dimensions of $260 \times 165 \times 140$ mm. To further simplify object division and analysis in the algorithm simulation, the block unit size is set to a cube with dimensions of $140 \times 140 \times 140$ mm.

Based on the block division method, when the bounding box size of an object is larger than the size of the basic block unit, it needs to be divided into smaller blocks. The bounding box is divided into cubes (Figure 3-9). The size of these cubes is defined by the measuring volume (MV) of the sensor lens used. When the bounding box size of an object is smaller than the size of the basic block unit, no further

division is required, and the bounding box dimensions can be directly used for generating candidate viewpoints.

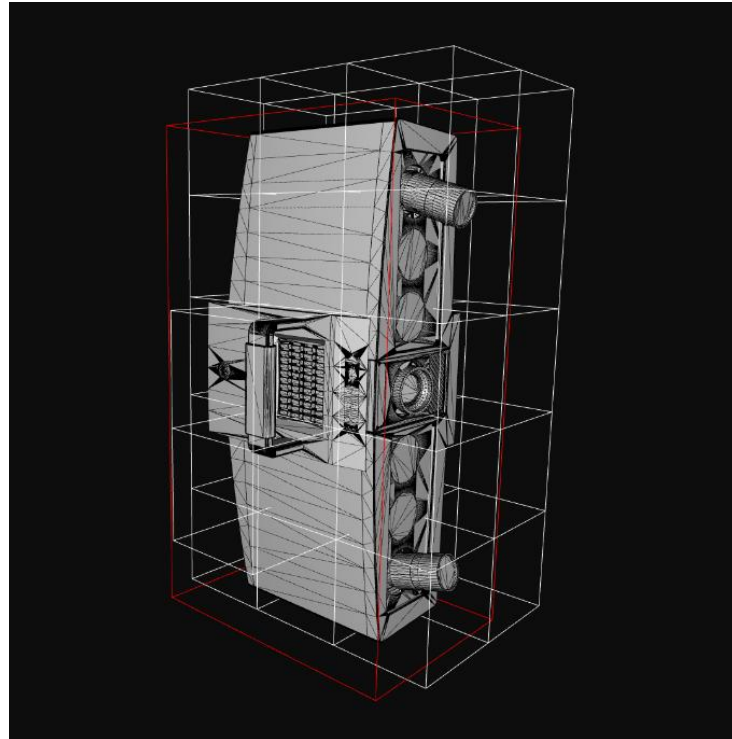


Figure 3-9: Block unit division for big object

3.1.3 Candidate Viewpoint Generation

In the optimal viewpoint selection algorithm, one crucial aspect is the generation of viewpoints. If the generated candidate viewpoints do not adequately cover the surface, it is impossible to approximate the true global optimal solution, and consequently, it is not feasible to derive a path that meets the scanning and reconstruction requirements. In this work, the generation of candidate viewpoints involves the following steps:

- First, we calculate the object's axis-aligned bounding box (AABB), determine the bounding box dimensions (length, width, height), and calculate the object's center. If the object's AABB dimensions are smaller than the block unit dimensions, we establish the ellipsoid parameters based on the bounding box dimensions. If the object's AABB dimensions are larger than the block unit dimensions, we establish the ellipsoid parameters based on the block unit dimensions.
- Then, based on the dimensions and spatial position of the AABB or block unit, we can define the semi-major axis lengths of the ellipsoid (a , b , c) and the center position of the ellipsoid (center) and set the interval angles for uniformly generating viewpoints.

- Next, we iterate through the zenith angles (θ) from the small angle step to π (180 degrees). For each zenith angle, we select an appropriate step size for the azimuth angle (ϕ) based on the angle range. If the zenith angle is within [0, 45] degrees or greater than 135 degrees, we use the large angle step; otherwise, we use the small angle step. For each azimuth angle, we calculate the x, y, z coordinates of the viewpoint and form a point.
- At last, we set the view direction as the vector pointing from the viewpoint to the center of the ellipsoid and normalize it. We classify the viewpoint based on the zenith and azimuth angles, and finally, add the viewpoint, view direction, and viewpoint category to the candidate viewpoint set.

Through this process, we can generate a set of viewpoints that cover the entire surface of the ellipsoid. These viewpoints can be effectively used for 3D scanning and reconstruction. The pseudocode for the generation process is as follows:

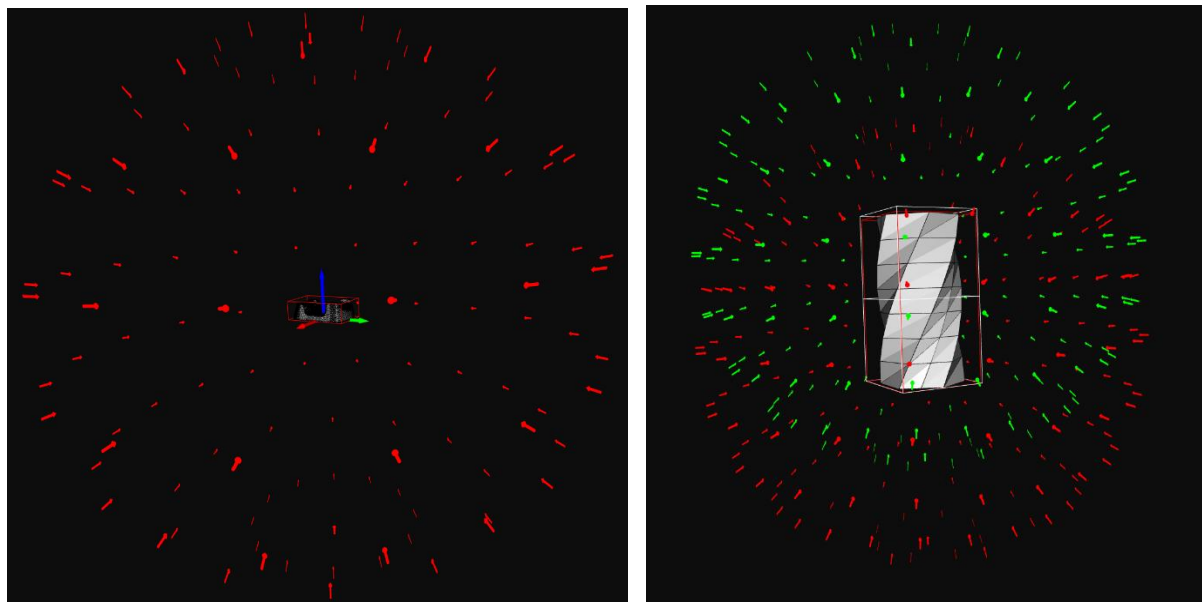
Table 3.1: Candidate Viewpoint Generation

Algorithm 1 Generating Candidate Viewpoints on an Ellipsoid	
Input:	Semi-major axis lengths of the ellipsoid along the x, y, and z axes (a, b, c); center coordinates of the ellipsoid (center); large angular interval (angle_step_large); small angular interval (angle_step_small)
Output:	Candidate viewpoint set (viewpoints)
	<ol style="list-style-type: none"> 1. Initialize an empty list for viewpoints. 2. Convert angle_step_large and angle_step_small from degrees to radians. 3. Add special cases for zenith and nadir points: <ol style="list-style-type: none"> 1. Append (center + [0, 0, c], [0, 0, -1], 'Topview') to viewpoints. 2. Append (center + [0, 0, -c], [0, 0, 1], 'Bottomview') to viewpoints. 4. For each zenith angle θ from angle_step_small to π with a step of angle_step_small: <ol style="list-style-type: none"> 1. If θ is within [0, 45] degrees or greater than 135 degrees: <ol style="list-style-type: none"> 1. Set angle_step_phi to angle_step_large. 2. Else: <ol style="list-style-type: none"> 1. Set angle_step_phi to angle_step_small. 3. For each azimuth angle ϕ from 0 to 2π with a step of angle_step_phi: <ol style="list-style-type: none"> 1. Compute $x = a * \sin(\theta) * \cos(\phi) + center[0]$. 2. Compute $y = b * \sin(\theta) * \sin(\phi) + center[1]$. 3. Compute $z = c * \cos(\theta) + center[2]$. 4. Form the point as [x, y, z]. 5. Calculate view direction as (center - point) normalized. 6. Classify the viewpoint based on θ and ϕ. 7. Append (point, direction_normalized, view) to viewpoints.

5. Return the viewpoints list.

To start with a 30-degree interval helps reduce the number of candidate viewpoints, thus saving computation time when calculating the measurement quality parameters of the candidate viewpoints. Special handling of viewpoints within the zenith angle range of 45 to 135 degrees is necessary because the lower the zenith angle, the greater the distance between each degree of azimuth angle. To ensure a more uniform spatial distribution of candidate viewpoints, lower latitude viewpoints need to be distributed at smaller azimuth angle intervals. This interval is suitable for reference models where the surface curvature does not undergo extreme changes.

Below is an example of generating candidate viewpoints for a given object, as shown in Figure 3-10. In Figure 3-10(a), the object bounding box's size is smaller than a block unit, so the generation of candidate viewpoints is only based on its bounding box's size. In Figure 3-10(b), the object is divided into two blocks, and the candidate viewpoints are generated based on the center of the two blocks, which are shown in different colors.



(a)Candidate viewpoints for small object (b)Candidate viewpoints for big object

Figure 3-10: Candidate viewpoints set

For a binocular structured light scanner to achieve 3D reconstruction, it must ensure that the projector can project the grating onto the surface of the object to be measured, and that the binocular cameras can capture the grating images. Therefore, in the candidate viewpoint generation process, it is necessary to determine not only the position and direction of the scanning viewpoints but also the pose in 3D space. The candidate viewpoint coordinate system is used to represent the viewpoint pose: the Z-axis points from the candidate viewpoint towards the center of the sphere, the X-axis is the tangent to the circular plane at the candidate viewpoint, and the Y-axis

is determined based on the right-hand rule. Due to the constraints of scanner stability, this experiment only considers the horizontal pose of the scanner (camera-projector) axis. The pose of the scanner is shown in Figure 3-11.

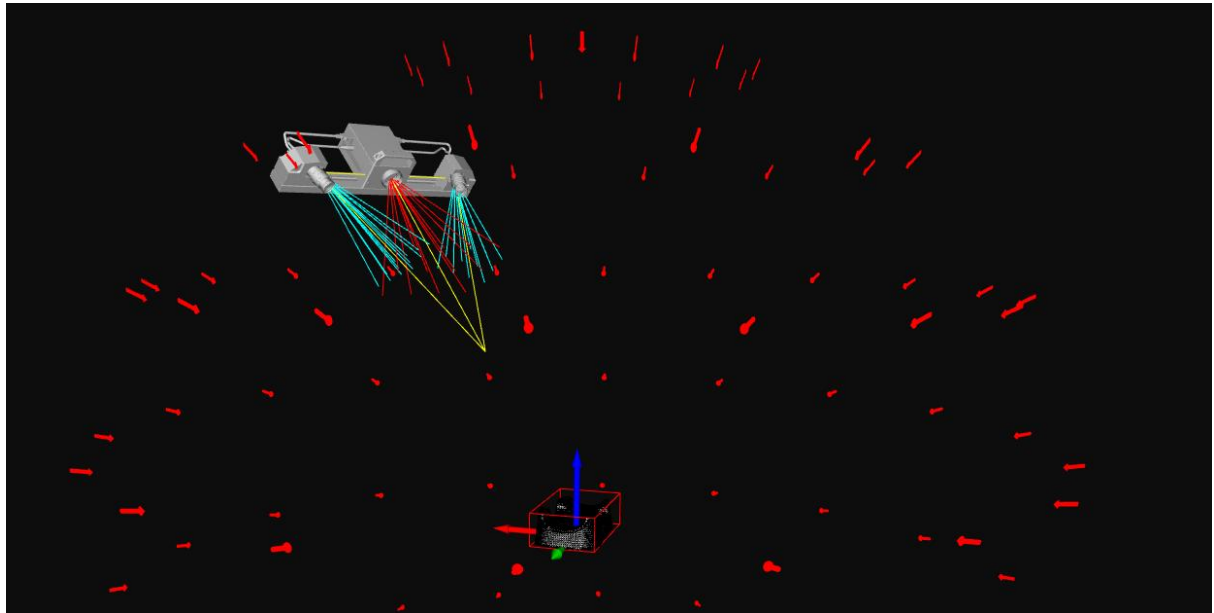


Figure 3-11: The pose of the scanner

Compared to methods like random sampling for viewpoint generation by Jing[8] or those based on the robot kinematic space, this viewpoint generation method is more computationally convenient and faster while achieving uniform distribution. By ensuring that each part of the object is entirely within the scanner's depth of field through block division, adjusting the viewpoint angle intervals to increase or decrease viewpoint density can achieve strong adaptability.

3.2 Optimal Viewpoint Selection Strategy

The focus of this section is on selecting the optimal set of viewpoints from a candidate set for scanning an object and subsequently generating a scanning path based on this selection. This subsection will detail the criteria and process for selecting the optimal viewpoints. The approach involves an iterative method where, in each iteration, a target function is used to calculate the score for each viewpoint. The highest-scoring viewpoint is selected, and this process continues until a preset goal is reached, ultimately yielding an optimal set of viewpoints.

3.2.1 Determining Measurement Constraints of the Scanner

Determining the measurable surface range of the object from a specified viewpoint is the prerequisite for evaluating viewpoint quality. This requires a comprehensive

consideration of the scanner's visibility constraints and occlusion constraints, which involves assessing whether the light from the projector can reach the object's surface unobstructed and return to the camera. Additionally, the angles of incidence of any light path from the projector to the surface must not be too steep, which would otherwise hinder image capture.

Based on the scanner's optical parameter constraints, such as the scanning distance and angle from the scanner to the object's surface features, we can evaluate the scanning quality of a specific feature from a given viewpoint. Generally, the further the object is from the optimal focus plane and the less directly it faces the scanner, the poorer the scanning quality will be. Therefore, the proposed optimal viewpoint selection strategy involves determining the effective measurement range and scanning quality of candidate viewpoints based on the scanner's visibility, occlusion, and optical parameter constraints. This strategy constructs an effective simulation environment and a viewpoint quality evaluation function.

3.2.1.1 Visibility Constraint Determination

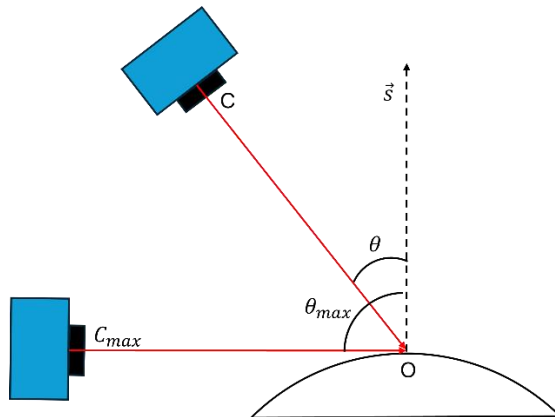


Figure 3-12: The visibility constraint of a single camera

Figure 3-12 illustrates the visibility of a single camera. The camera's optical center is defined as C , and a point on the object's surface is defined as O , with the normal vector at point O represented as \vec{s} . Generally, the angle θ between the optical axis vector and the surface normal vector s should be less than 90° to satisfy the visibility constraint. However, it has been observed that when the angle approaches 90° , the scanning quality deteriorates significantly, failing to meet image acquisition requirements. Therefore, a threshold value θ_{max} is set to filter the scanned surface patches and light rays, with θ_{max} set to 85° based on the scanner's optical and algorithmic design information. The visibility constraint for a single camera must satisfy the following equation:

$$\theta = \cos^{-1} \left(\frac{\overrightarrow{OC} * \vec{s}}{\|\overrightarrow{OC}\| * \|\vec{s}\|} \right) \leq \theta_{max}$$

Figure 3-13 illustrates the visibility constraint for a binocular structured light scanner, where P is the optical center of the projector. The actual visible area of the binocular structured light scanner is determined by calculating the visible areas of each camera and the projectable area of the projector, then taking their intersection. The projectable area of the projector also follows the visibility constraint determination due to the involvement of light incidence and reflection issues. However, based on empirical data, the visibility threshold θ_{max} for the projector is generally 5-10 degrees smaller than that of the cameras.

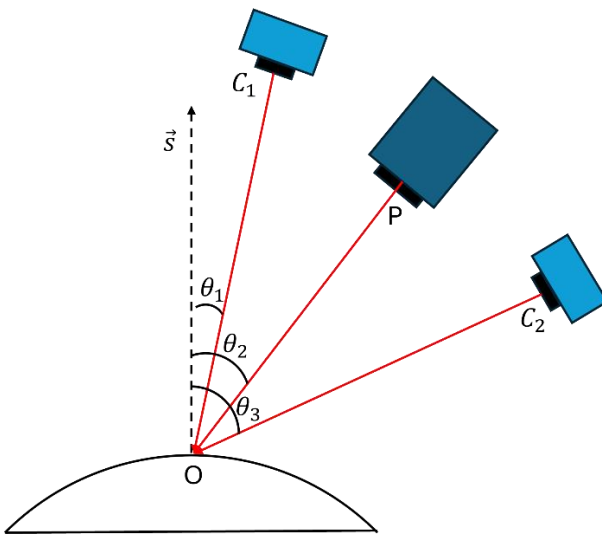


Figure 3-13:The visibility constraint for a binocular structured light scanner

3.2.1.2 Occlusion Constraint Determination

When attempting to view a feature of an object from a particular viewpoint, some or all points of the feature may not be visible. This can occur for the following reasons: the feature is occluded either by some part of the object on which it lies or by other objects in the environment. This occlusion happens when a ray emanating from the viewpoint and directed towards a point on the feature is obstructed by the boundary of an object, assuming the objects are opaque. When the object causing the occlusion is the same as the one on which the feature lies, this is termed self-occlusion.

Thus, determining the occlusion constraint essentially involves checking whether a ray intersects multiple surface patches. During ray casting simulation, if a ray intersects the object at a point A_1 , and the distance from the ray's origin to this intersection point is less than the distance from the ray's origin to the target triangle A_0 , it can be concluded that the ray is occluded by other parts of the object and

cannot successfully reach the target triangle. This is the core idea behind the Möller-Trumbore algorithm.

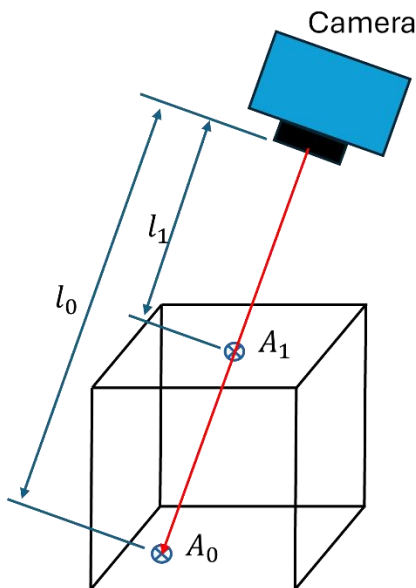


Figure 3-14: Occlusion Constraint Determination

The Möller–Trumbore ray-triangle intersection algorithm[21], named after its inventors Tomas Möller and Ben Trumbore, is a fast method for calculating the intersection of a ray and a triangle in three dimensions without needing precomputation of the plane equation of the triangle. This algorithm is commonly used in computer graphics to implement ray tracing computations involving triangle meshes.

Thanks to advances in computational power, it is now possible to use more detailed ray casting algorithms for occlusion constraint determination without having to simplify calculations through down-sampling, which was difficult in previous studies. To accelerate computations, I used the Bounding Volume Hierarchy (BVH) based on AABB (Axis-Aligned Bounding Box) trees, commonly employed in collision detection in physics engines like Bullet and Havok. This structure divides and stores the object's AABB shape, and its property (non-collision between different parent bounding boxes) allows for the rapid filtering of many unlikely collision pairs, optimizing the ray casting function and significantly speeding up the ray-triangle intersection tests.

However, limited by computational performance and algorithmic efficiency considerations, the number of rays simulated in my ray casting algorithm remains finite. Generally, when dealing with highly detailed models, $3 \times 4000 \times 3036$ rays are used for each viewpoint, meaning each viewpoint casts 36 million rays in the given direction towards the target area of the object during occlusion constraint

determination. Only when rays emitted from both the projector and the two cameras hit a surface patch without obstruction is the patch marked as visible. This process effectively takes the intersection of the visible areas of the two cameras and the projectable area of the projector. After performing visibility constraint determination and filtering, the algorithm records each hit triangle and the rays that hit it without duplication for further optical parameter constraint determination.

3.2.1.3 Optical Parameter Constraint Determination

Structured light 3D scanners offer high scanning precision. However, if we aim to use this 3D data for high-precision applications (such as inspection tasks), it is crucial to capture the 3D points under optimal precision conditions. When obtaining the 3D point cloud data of parts, various sources of error can alter the measurements. The most significant factors include the distance between the sensor and the surface to be scanned, the angle of incidence relative to the surface, the brightness of the projector and ambient light, and the material and color of the object's surface. For quantifiable considerations, the optimal viewpoint selection algorithm designed in this study mainly focuses on the distance between the sensor and the surface to be scanned and the angle of incidence relative to the surface.

Based on the law of reflection, to ensure that the light projected onto the object's surface by the projector is received with high quality by both cameras on either side after reflection, the angles between the optical axes of the projector and the two cameras and the surface normal vector must be within a certain range. Otherwise, the structured light projected by the projector may not be received by one of the cameras due to visibility constraints, or the reflected light's intensity may be too low, resulting in a low signal-to-noise ratio. Since the raster images projected by the 3D structured light scanner's projector contain a large amount of information, the requirements for the reflection angle are higher. Therefore, determining the optical parameter constraints during viewpoint selection is crucial. Based on the imaging principles of cameras, they always come into sharp focus precisely at the best-focused point and gradually come into and out of focus around a threshold. Hence, the distance of the object surface from the camera's optimal focus point significantly affects the scanning quality.

Prieto [22] demonstrated that when the angle between the surface normal and sensor orientation exceeds 35° , the resulting point cloud is extremely noisy and cannot obtain accurate measurements. Prieto[23] also modeled the noise of 3D measurement points mathematically and validated the noise characteristics introduced at each 3D measurement point in the form of a covariance matrix, showing a relationship with the sensor-to-surface distance and the angle of incidence between the light beam and the surface normal. With a fixed sensor distance, increasing the angle of incidence β results in exponentially increasing noise characteristics. Therefore, smaller angles of incidence produce less noise, indicating that the sensor should be placed as perpendicular to the surface as possible.

Conversely, with a fixed angle of incidence β , changing the sensor-to-surface distance determines the covariance matrix for the parameter d, presenting a typical U-shaped variance curve. The variance decreases and then increases with distance d, with the minimum measurement variance occurring near the optimal focus distance, where data accuracy is highest on the focal plane.

Based on current research, this study introduces the distance from the sensor to the surface triangle and the angle between the incident light and the normal of the surface triangle as imaging quality parameters in the viewpoint quality evaluation function. The area of the surface triangle is used as a weight for weighted summation, evaluating the imaging quality of each viewpoint.

3.2.2 Optimal Viewpoint Selection

The core of viewpoint planning is optimal viewpoint selection, which aims to minimize the number of viewpoints while ensuring the quality and completeness of the model scan, thereby improving scanning efficiency. When constructing the viewpoint quality evaluation function, it is essential to consider both the surface coverage of the model and the scanning quality of the model surface. The former ensures that as many triangles as possible are included under a single viewpoint, while the latter analyzes the scanning quality to ensure that features are captured effectively.

The principle of the viewpoint quality evaluation function used in this study is as follows. To ensure an increase in the surface coverage of the model, when a surface patch with an area S_i is scanned, it receives a basic score $a * S_i$. For the model surface scanning quality evaluation, the scanning quality of the surface patch is analyzed. High scanning-quality will result in a bonus, while poor scanning quality will result in a penalty. Both the bonus and penalty are weighted by the area S_i of the surface patch. The total quality score for a viewpoint is obtained by summing the basic scores and quality scores of all the surface patches that can be scanned from that viewpoint.

The viewpoint quality evaluation function based on this principle is constructed as follows:

$$G_v = a * G_c + b * G_q$$

where:

- G_v is the total score of the viewpoint.
- G_c is the coverage score of the viewpoint.
- G_q is the quality score of the viewpoint.

- a, b are weighting coefficients used to set the weight of scanning coverage and scanning quality

The coverage score of a single viewpoint is equal to the sum of the areas of all the triangular patches it can scan, expressed as:

$$G_c = \sum_{i=0}^n S_i$$

where:

- S_i is the area of the i -th triangular patch
- n is the number of surface patches that been scanned

The quality score incorporates the distance from the sensor to the surface triangle and the angle of incidence relative to the surface triangle's normal into the viewpoint quality evaluation function. This score is also weighted by the area of the corresponding surface patch, expressed as:

$$G_q = \sum_{i=0}^n S_i * (c * Q_\delta(i) + d * Q_{dis}(i))$$

where:

- $Q_\delta(i)$ is the quality score based on the angle of incidence relative to the surface triangle's normal.
- $Q_{dis}(i)$ is the quality score based on the distance from the sensor to the surface triangle.
- c, d are weighting coefficients used to set the weight of $Q_\delta(i)$ and $Q_{dis}(i)$.
- $Q_\delta(i)$ and $Q_{dis}(i)$ can be expressed as:

$$Q_\delta(i) = 1 - \frac{2 * \delta_i}{\delta_{max}}$$

$$Q_{dis}(i) = 1 - \frac{2 * |l_i - F|}{D}$$

where:

- δ_i is the angle between the optical axis vector of the viewpoint and the normal vector of the i -th surface patch.

- l_i is the distance from the sensor to the surface triangle.
- δ_{max} is the maximum angle could exist after filter between the optical axis vector of the viewpoint and the normal vector of the i -th surface patch.
- F is the best focal length of the scanner, D is the depth of field (DOF)

The structured light scanning viewpoint planning process is illustrated in Table 3.2, and the main steps are as follows:

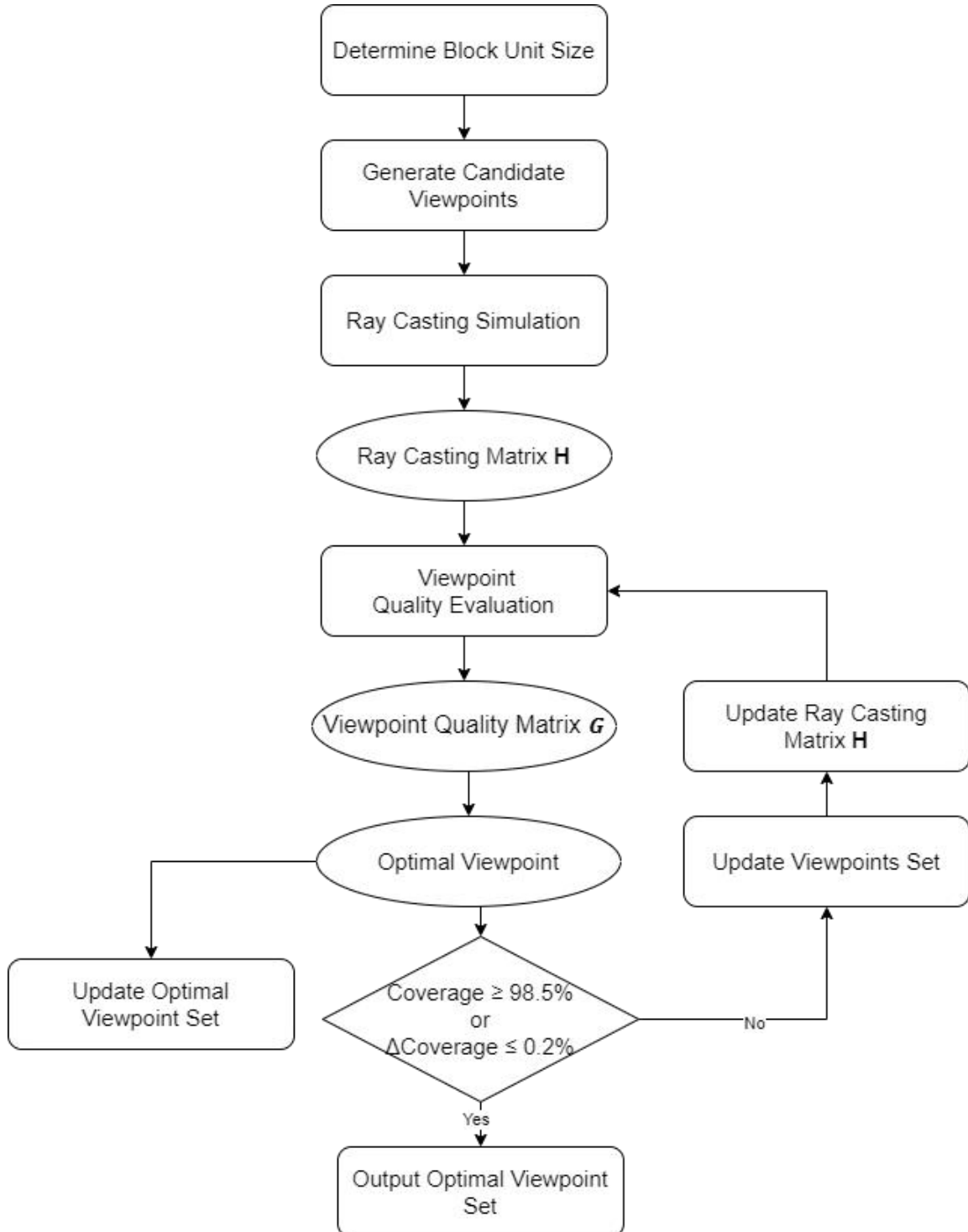


Figure 3-15: Procedure of Optimal Viewpoint Selection

- **Step 1:** Determine the block unit size based on the optical parameter constraints of the 3D scanner. Then, use these blocks to partition the model for each object to be scanned.
- **Step 2:** For a given model, generate a candidate viewpoint set on the ellipsoidal measurement space based on the dimensions and spatial position of the bounding box or block unit at given intervals. Pre-filter the viewpoints that do not meet the experimental platform and fixture conditions.
- **Step 3:** For each viewpoint, perform ray casting simulation. Evaluate all surface voxel grids using optical parameter constraints, visibility constraints, and occlusion constraints to determine the set of surface patches each viewpoint can scan. Establish a relationship matrix H between candidate viewpoints and surface patches.
- **Step 4:** For each viewpoint in the candidate viewpoint set, calculate the scanning coverage and data quality of the model based on the viewpoint quality evaluation function. Construct the viewpoint quality matrix G , record the quality of each point, and select the viewpoint with the highest quality score as the optimal viewpoint. Output this to the optimal viewpoint set.
- **Step 5:** Remove the current optimal viewpoint from the candidate viewpoint set. Mark the surface patches scanned by the current viewpoint to exclude them from the next iteration's viewpoint quality evaluation, but still include them in occlusion constraint determination. Then, repeat Steps 3 and 4.
- **Step 6:** After each iteration, check if the current scanning result of the model surface meets the desired level (e.g., scanning coverage reaches 98.5% of the total surface area). If the coverage target is achieved or no further improvement in coverage is detected, terminate the process.

3.3 Determination of Key Algorithm Parameters

The choice of weight coefficients in the viewpoint quality evaluation function affects the tendency of viewpoint generation, and consequently impacts the model scanning time and quality. When the weight coefficient for scanning coverage is reduced, the viewpoint quality evaluation function focuses more on the scanning quality of the viewpoint rather than the coverage area. This increases the number of viewpoints required to achieve the same scanning coverage. Once all high-quality surface patches are scanned, the iterative algorithm may conservatively choose not to scan any patches to avoid penalties, leading to longer actual scanning times for the robot.

Conversely, when the weight coefficient for imaging quality is reduced, the viewpoint quality evaluation function emphasizes the area that a viewpoint can scan rather than

the scanning quality. This results in fewer viewpoints needed to achieve the same scanning coverage, reducing the actual scanning time of the robot. However, the corresponding scanning quality will be poorer, with decreased accuracy, increased scanning noise, degraded surface reconstruction quality, and ineffective capture of features in regions with significant curvature changes.

To ensure both high scanning quality and a reduced number of viewpoints, it is necessary to qualitatively analyze and test the weight coefficients in the viewpoint quality evaluation function. This chapter will focus on studying the impact of the weight coefficients a and b (the weights for scanning coverage and imaging quality) on the scanning results. Other parameters, as well as the weight coefficients e and f , will remain unchanged based on the control variable method. In practice, it has been observed that the scanning angle has a greater impact on scanning quality compared to scanning distance. Therefore, based on empirical data, the weight coefficients for scanning angle and scanning distance are set to $e=0.6$ and $f=0.4$.

The following graph shows the relationship between the number of viewpoints and scanning coverage for the Pikachu model. Analyzing the overall trend, the scanning integrity rapidly increases with the number of viewpoints across all five weight coefficients. The increase rate slows down after reaching 90% coverage and gradually stabilizes around 97%. When the weight coefficient a is greater than 0.25, the curves stabilize earlier and achieve higher scanning integrity. With eight viewpoints, the scanning coverage for different weight coefficients is 98.80%, 97.90%, 97.67%, 97.54%, and 96.14%, respectively. Therefore, considering both scanning speed and final coverage, the value of weight coefficient a should be greater than or equal to 0.25.

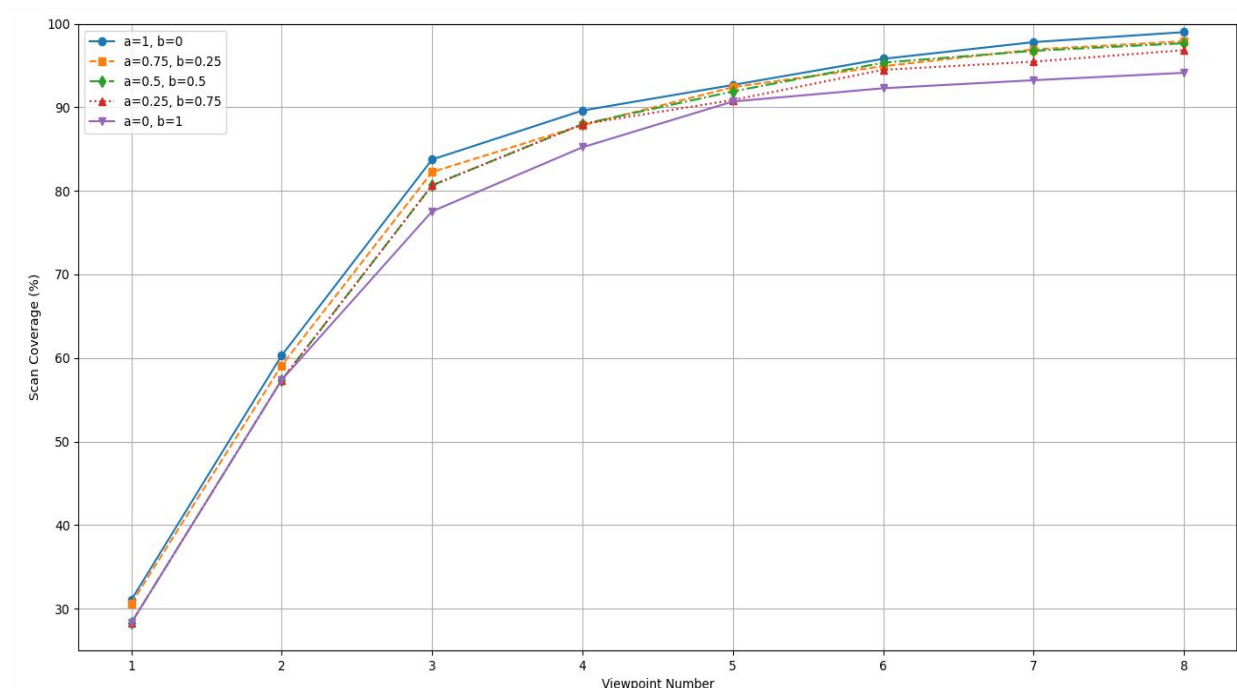


Figure 3-16: Relationship between the number of viewpoints and scanning coverage under different weight coefficient

The evaluation of the scanning quality of the surface patches is based on the following formula:

$$Q(i) = Q_{\delta}(i) + Q_{dis}(i)$$

Based on the value range of this formula (-1, 1), we can categorize surface patches into four grades: A (Excellent) for (0.5, 1), B (Good) for (0, 0.5), C (Average) for (-0.5, 0), and D (Poor) for (-1, -0.5). The quality distribution of surface patches scanned with eight viewpoints under different weight coefficients is shown in Table 3.4.

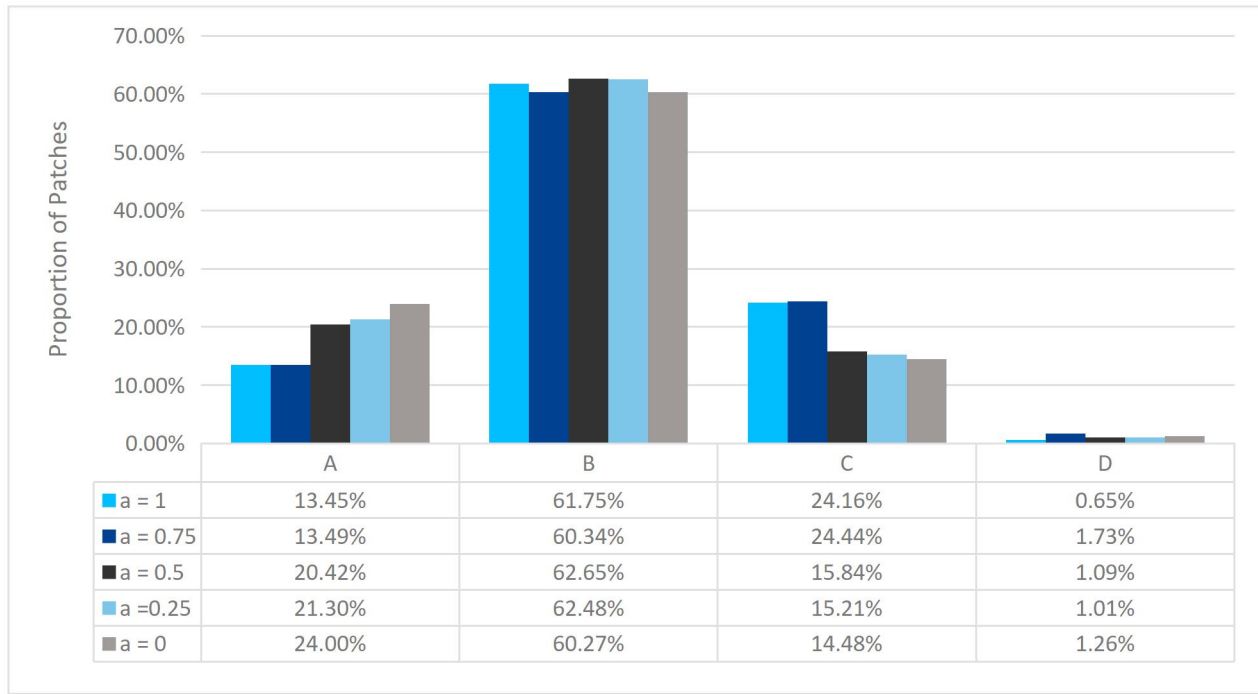


Figure 3-17: The quality distribution of surface patches under different weight coefficients

It is evident that as the weight coefficient a decreases, the proportion of surface patches with A-grade scanning quality increases, while the proportion of C and D-grade patches decreases. When a is less than 0.5, the proportion of A-grade patches reaches 20%, and the proportion of C-grade patches remains around 15%, significantly better than schemes with $a \geq 0.75$. According to Table 3-2, the weight coefficient a should be less than or equal to 0.5.

Based on the above analysis, for the Pikachu model, the weight coefficient a should be either 0.5 or 0.25. From the perspective of scanning quality, the proportion of excellent patches is 21.30% when $a=0.25$ and 20.42% when $a=0.5$, a difference of only 0.88%. However, considering scanning coverage and speed, the scheme with

$a=0.5$ offers higher scanning efficiency. Therefore, to balance scanning coverage and quality, the selected weight coefficients are $a=0.5$ and $b=0.5$.

4 Complex Surface Model Measurement Experiment

4.1 Experimental Setup

4.1.1 Design of the Automated 3D Reconstruction System

This study developed an automated measurement system for complex surfaces, as shown in Figure 4-1. The system uses a structured light projector and high-precision industrial cameras mounted on a multi-axis robotic arm, combined with a rotary table to form the 3D measurement system. During operation, the system first performs viewpoint planning for the unknown object, determining the positions and sight directions of multiple sensor viewpoints. These viewpoints are then converted into the robotic arm's poses and rotary table angles. The system optimizes the path to achieve the shortest distance and sorts the viewpoints to generate an optimal path. Finally, the robotic arm's movement and the rotary table's rotation are synchronized through code to perform automated 3D scanning, resulting in the acquisition of a complete 3D model.

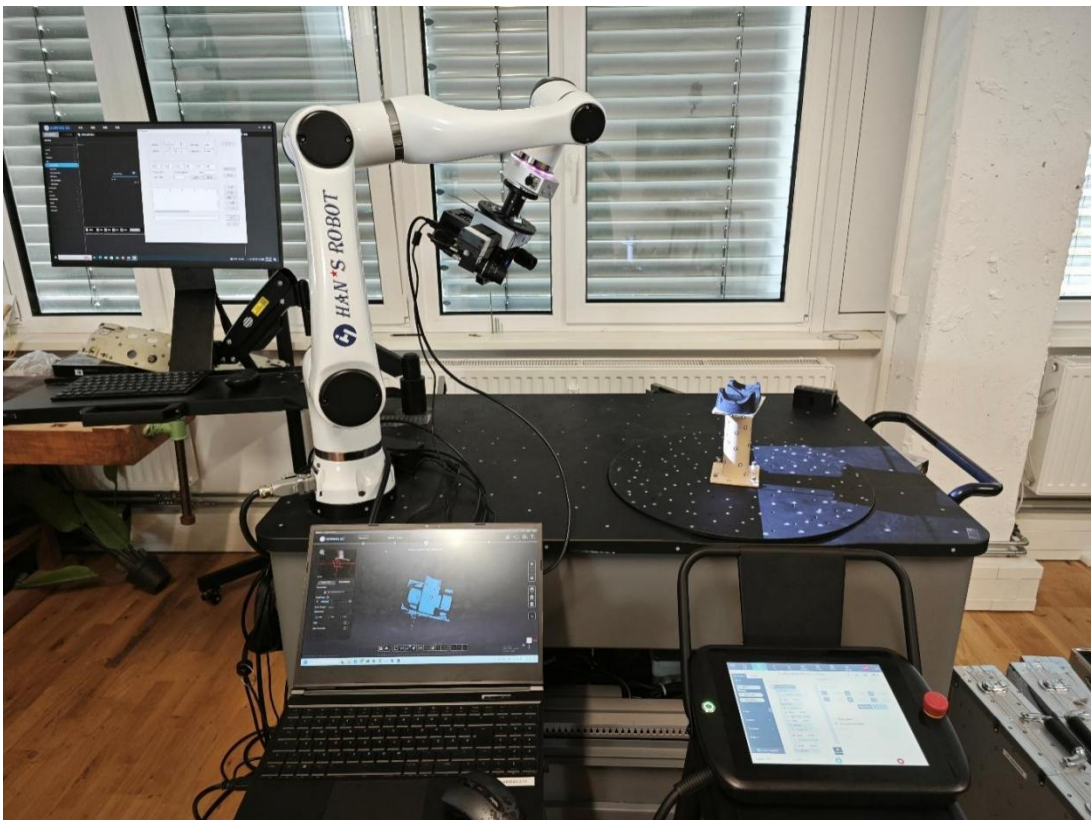


Figure 4-1: Setup of automated measurement system

Considering the difficulties in scanning complex workpieces and the limitations of the scanner's field of view and range, the system controls the robotic arm to move the scanner along the scanning path while also controlling the high-precision rotary table to rotate the workpiece. This approach allows for capturing images of the workpiece from multiple angles, enhancing the completeness of the reconstruction. A control box coordinates the rotary table and assists the robot, while a high-performance computer processes the scanning information.

The entire measurement process involves changing the 3D sensor's viewing angle by controlling the rotary motor and the robotic arm. The robotic arm used is the E05 collaborative robot from Han's, the rotary table is from Panasonic, and the structured light scanner is the TranscanC from Shining 3D. The scanner consists of two high-precision industrial cameras and a structured light projector, achieving a reconstruction accuracy of up to 0.05 mm, which meets the experimental requirements. The specific parameters of Robot Arm, Turntable and Structured Light Scanner are listed in the Table 4.1- Table 4.3 below:

Table 4.1: Parameters of Robot Arm

Model Name	Han's E05
Type	Robot Arm
Axes	6
Payload	5.0 kg
Reach	800 mm
Repeatability	±0.02mm
Weight	25 kg
Joint Range	J1/4/6: ±360° J2: ±135° J3: ±153° J5: ±180°
Joint Speed	J1-J4: 180°/s J5-J6: 200°/s

Table 4.2: Parameters of of Turntable

Model Name	Panasonic MINAS A6
Motor Name	MSMF042L1V2M
Motor Type	Servo Motor
Motor Output	400W
Continuous stall torque (N · m)	1.27
Rated rotational Max. speed (r/min)	6000
Turntable Diameter(mm)	500

Table 4.3: Parameters of of Structured Light Scanner

Model Name	Shining3d Transcan C
Light Source	White LED Light
Scan Mode	Structured-light scan
Calibration Mode	Manual calibration
Scan Range	150 mm x 96 mm/ 300 mm x 190 mm
Single Shot Accuracy	0.035 mm
Working Distance	260 mm/ 480 mm
Point Distance	0.0375 mm; 0.075 mm; 0.114 mm
Weight	2.7 KG (Net weight of host module)

4.1.2 Calibration of the Automated 3D Reconstruction System

Before conducting the actual scanning experiments, it is necessary to calibrate the automated 3D reconstruction system. The primary considerations for calibration are as follows:

- **Ensure Accuracy:** Calibration ensures the measurement accuracy of the optical system. The core of the 3D reconstruction system is the scanner's ability to accurately capture and reconstruct the surface details of objects. Through calibration, any potential errors in the system can be corrected, establishing the

correspondence between image points and spatial object points, thus ensuring high precision in the scan data.

- **Eliminate System Errors:** All optical equipment, robotic arms, and rotary tables have inherent system errors. Calibration identifies and corrects these errors, such as camera perspective distortion, projector non-linearity, and robotic arm positioning errors.
- **Unify Coordinate Systems:** The calibration process unifies the coordinate systems of all devices (cameras, projectors, robotic arms, rotary tables) into a global coordinate system. This involves determining the transformation matrix between the 3D scanner and the robotic arm, as well as the transformation matrix between the rotary motor's axis coordinates and the robotic arm's coordinates, establishing the transformation relationships of each module's coordinates to the world coordinate system. This is crucial for precise calculation and control of the relative positions and orientations of all devices.
- **Optimize Scanning Path:** After calibration, the system has a better understanding of the position and direction of each viewpoint, allowing for more efficient planning of the scanning path, reducing redundant movements, and improving scanning efficiency.
- **Improve Data Consistency:** Calibration ensures consistency in the scan data from different viewpoints and angles, which is essential for subsequent data stitching and 3D model reconstruction.

Specifically, the calibration process of the 3D reconstruction system generally includes the following aspects:

- **Camera Calibration:** Determining the internal parameters of the camera (such as focal length, principal point, distortion coefficients) and external parameters (camera position and orientation in space).
- **Projector Calibration:** Determining the projection characteristics of the projector and its relative position to the camera.
- **Robotic Arm Calibration:** Determining the motion precision and repeatable positioning accuracy of the robotic arm.
- **Overall System Calibration:** Combining the calibration results of all devices to ensure the coordination and unification of the entire system during operation.

Due to constraints, direct calibration of the robotic arm is not feasible, and the manufacturer's provided coordinate transformation functions will be used for converting between the robotic arm's base coordinates and TCP (Tool Center Point) coordinates. The calibration process provided by Shining3D for the 3D scanner includes camera and projector calibration, thus the system calibration involves two main steps:

- (1) Optical calibration of the 3D scanner.
- (2) Calibration of the transformation relationships between the coordinate systems of the 3D reconstruction system.

4.1.2.1 Optical Calibration of the 3D Scanner

Cameras are the fundamental units of a 3D measurement system. Before performing 3D reconstruction of an object, it is essential to establish the correspondence between image points and spatial object points. This involves determining the transformation matrix between the camera coordinate system and the world coordinate system (external parameters) and the camera's intrinsic parameters (internal parameters), a process known as camera calibration. High precision is required in the field of 3D measurement, so metric calibration is typically used. The camera calibration process generally involves these steps:

Capture Images: Take multiple images of the calibration target from different angles and orientations.

Identify Reference Points: Detect and encode reference points on the calibration target in each image.

Initial Parameter Estimation: Use a linear model to estimate initial intrinsic and extrinsic parameters, ignoring distortion.

Non-linear Optimization: Incorporate lens distortion and refine parameter estimates by minimizing reprojection error using non-linear optimization techniques.

Through these steps, the calibration process establishes a precise mathematical model of the camera, which is crucial for accurate 3D reconstruction. By accurately determining the intrinsic and extrinsic parameters, the system can precisely map the image coordinates to real-world coordinates, ensuring high accuracy in the 3D measurements.

The calibration process can be mathematically explained as follows[24]: A 2D point is represented by $m = [u, v]^T$, and a 3D point is denoted by $M = [X, Y, Z]^T$. To facilitate the calculations, we use \tilde{x} to denote the augmented vector by adding 1 as the last element: $\tilde{m} = [u, v, 1]^T$ and $\tilde{M} = [X, Y, Z, 1]^T$. The camera is modeled using the standard pinhole camera model. The relationship between a 3D point M and its 2D image projection m (perspective projection) is expressed by the following equation:

$$s\tilde{m} = A[R \ t]\tilde{M}$$

With

$$A = \begin{bmatrix} \alpha & \gamma & u_0 \\ 0 & \beta & v_0 \\ 0 & 0 & 1 \end{bmatrix}$$

Here, s is an arbitrary scale factor. The matrix (R, t) known as the extrinsic parameters, represents the rotation and translation that relate the world coordinate system to the camera coordinate system. The matrix A , known as the camera intrinsic matrix, contains the intrinsic parameters of the camera. In this matrix, (u_0, v_0) are the coordinates of the principal point, α and β are the scale factors along the image u and v axes, and γ describes the skewness between these two axes. The objective of camera calibration is to determine these five intrinsic parameters. For convenience, we use the notation A^{-T} to represent $(A^{-1})^T$ or $(A^T)^{-1}$.

The calibration process involves capturing multiple images and solving this set of equations simultaneously, as illustrated in the Figure 4-2 below.

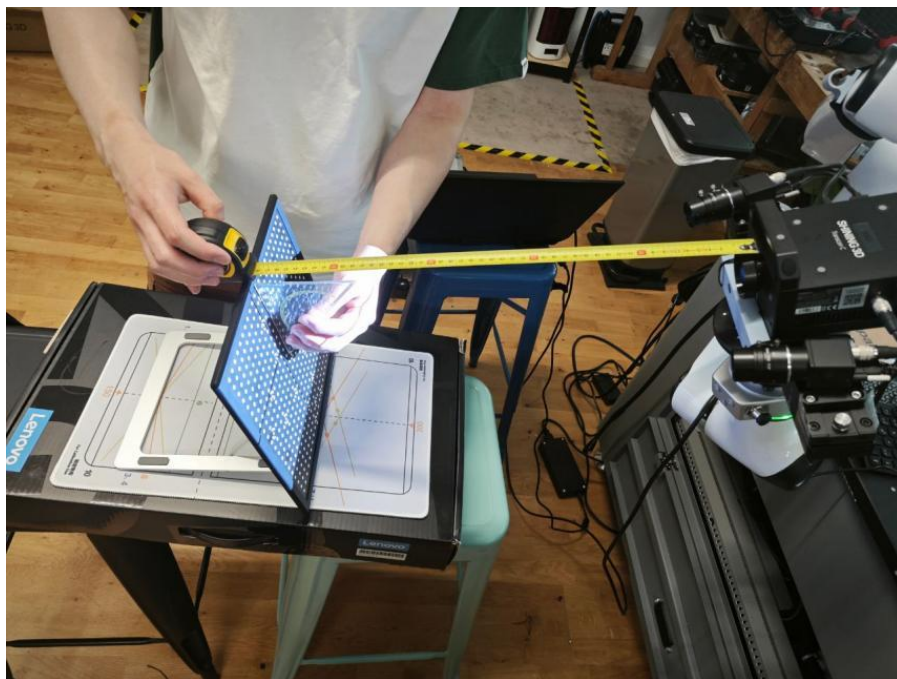


Figure 4-2: The calibration of the 3D Scanner

The calibration information of the cameras is as follows (units in pixels):

Table 4.4: Calibration information of left camera

Focal Length	$fc = \begin{bmatrix} 6668.08312 & 6667.42465 \\ 0.00000 & 0.00000 \end{bmatrix}$
Principal Point	$cc = \begin{bmatrix} 1939.53554 & 1471.63556 \\ 0.00000 & 0.00000 \end{bmatrix}$
Alpha	$\alpha = \begin{bmatrix} -0.000153 \\ 0.000000 \end{bmatrix}$
Distortion	$kc = \begin{bmatrix} -0.04359 & 0.34600 & -0.00209 & -0.00112 & -0.24560 \\ 0.00000 & 0.00000 & 0.00000 & 0.00000 & 0.00000 \end{bmatrix}$

Translation Vector	$T = [0.42910 \quad 1.40557 \quad 558.72951]$
Rotation Matrix	$R = \begin{bmatrix} 0.98495 & -0.01265 & 0.17236 \\ -0.00608 & -0.99923 & -0.03854 \\ 0.17272 & 0.03691 & -0.98427 \end{bmatrix}$

Table 4.5: Calibration information of right camera

Focal Length	$f_c = \begin{bmatrix} 6667.54259 & 6668.18595 \\ 0.00000 & 0.00000 \end{bmatrix}$
Principal Point	$c_c = \begin{bmatrix} 1972.47889 & 1587.87192 \\ 0.00000 & 0.00000 \end{bmatrix}$
Alpha	$\alpha = \begin{bmatrix} 0.000093 \\ 0.000000 \end{bmatrix}$
Distortion	$k_c = \begin{bmatrix} -0.02110 & 0.06457 & -0.00094 & 0.00093 & 1.13432 \\ 0.00000 & 0.00000 & 0.00000 & 0.00000 & 0.00000 \end{bmatrix}$
Translation Vector	$T = [-1.69264 \quad -7.15918 \quad 566.12879]$
Rotation Matrix	$R = \begin{bmatrix} 0.98034 & -0.00948 & -0.19708 \\ -0.01441 & -0.99961 & -0.02360 \\ -0.19678 & 0.02598 & -0.98010 \end{bmatrix}$

After the scanner calibration is completed, the calibration information can be used to adjust the ray casting simulation environment to achieve a simulation effect consistent with the actual scanner projection parameters. The Figure 4-3 below shows the process of validating the ray casting effect in the simulation environment. The simulated scanner projects three beams with different parameters onto a plane from a height of 480mm to simulate the light paths of two cameras and one projector. The intersection of these beams represents the actual visible area. The visible area obtained from the simulated projection, measured using the scale, is a 190*300mm rectangle. This matches the size observed in actual projection tests, thereby confirming the correctness of the simulation parameter settings.

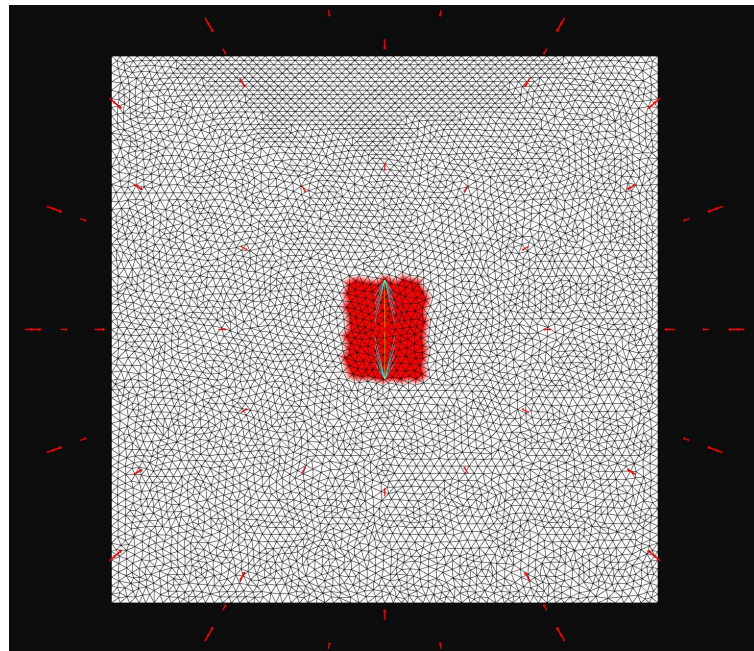


Figure 4-3: Validation of the ray casting effect in simulation environment

4.1.2.2 Overall System Calibration

The calibration of the turntable and robotic arm is crucial for the proper functioning of the entire measurement platform. The primary goal of rotary table calibration is to determine its rotational axis's spatial coordinate system and its relationship with the robotic arm's base coordinate system. Accurate calibration ensures that the rotary table's angular positions align precisely with the robotic arm's movements, thereby maintaining the scanning process's accuracy and consistency.

The calibration of the robotic arm involves determining the positions and angles of its joints to enable precise execution of scanning tasks. Due to practical constraints, this study uses the simulation model provided by Han's Robot Company, performing simulations in RobotDK to achieve the conversion between the robotic arm's base coordinates and flange coordinates.

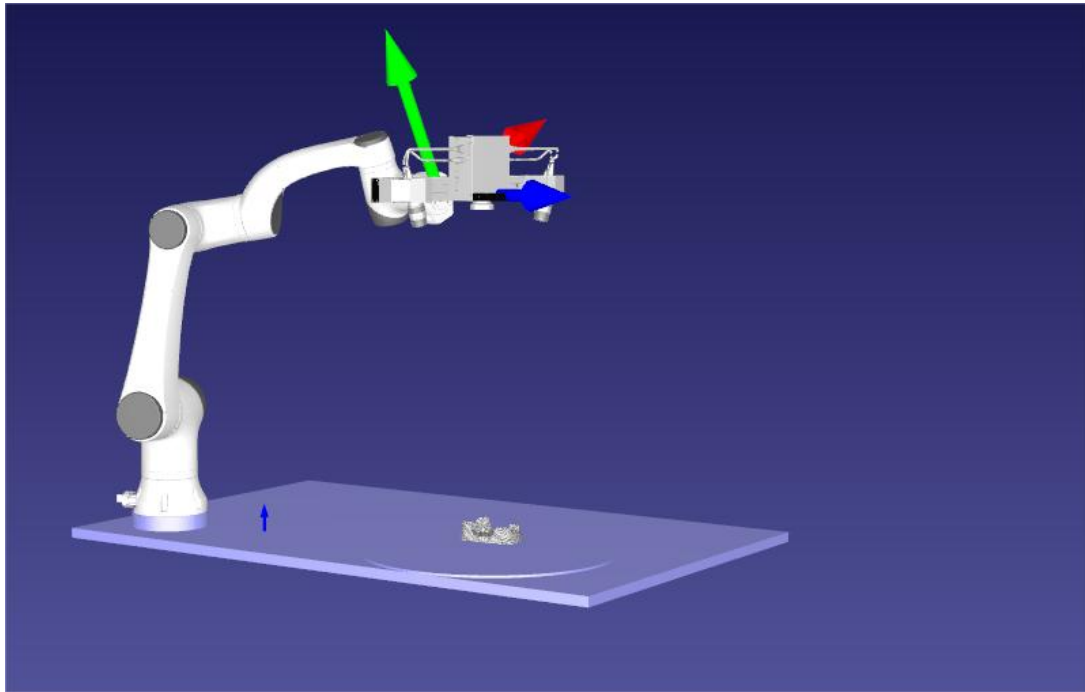


Figure 4-4: The calibration of the system in RobotDK

For viewpoints derived through iterative processes in the simulation environment, their coordinates and directions need to be converted into coordinate information that the robotic arm and rotary table can interpret. This requires understanding the corresponding coordinate relationships between the scanner and the robotic arm's end, as well as between the robotic arm and the rotary table's rotational axis. The mathematical model for solving these coordinate relationships can be expressed as $AX = XB$, where the transformation matrix X is given by:

$$X = \begin{bmatrix} R & T \\ 0 & 1 \end{bmatrix}$$

Here, R is the rotation matrix, and T is the translation vector. Only by determining the viewpoint coordinates based on the robotic arm's base or flange coordinate system can the viewpoint information be converted into the commands required by the robotic arm (such as (X, Y, Z, R_x, R_y, R_z) or $(J_1, J_2, J_3, J_4, J_5, J_6)$).

The basic principle involves fixing a camera at the robotic arm's end, moving the robotic arm to capture data from various target positions, and solving the transformation matrix between the camera and the robotic arm's end based on the robotic arm's positional data.

Traditionally, automated 3D reconstruction systems or other applications requiring precise tool operations via robotic arms employ the hand-eye calibration method for overall system calibration. This method involves using calibration targets (such as circular markers or checkerboards). During calibration, the robotic arm moves the camera to capture the target at different positions. Traditional methods are then used to compute the camera's external parameters, followed by calculating the hand-eye matrix using the robotic arm's motion parameters.

However, in this experiment, a high-precision scanner is used to scan the entire experimental platform from different positions. By utilizing Geometry ControlX in combination with RobotDK software, we determine the spatial relationship between the rotary table's rotational axis and the robotic arm's base coordinate system, as well as the relationship between the 3D scanner's external parameters and the robotic arm's flange coordinate system. Continuous fine-tuning of the robotic arm's TCP (X, Y, Z, R_x, R_y, R_z) and comparison with simulation results allow us to obtain a hand-eye matrix within an acceptable accuracy range.

For further calibration, we perform an additional calibration before each use. This involves aligning the scanner's optical center with the rotary table's central axis in a vertical position, reading the robotic arm's pose, and comparing it with the simulation environment's parameters. A compensation value is calculated and inputted to ensure the scanning path's accuracy. Through these methods, we achieve a highly accurate calibration of the automated 3D inspection platform. Experimental validation confirms that during the entire scanning path, the scanner's optical axis maintains a projection angle deviation of less than 1° from the designed angle, ensuring the system's overall measurement accuracy and stability.

4.2 Analysis of Scanning Results

4.2.1 Comparison of Single Frame Point Clouds

When using a 3D scanner to obtain point cloud data of parts, several sources of error can impact the measurement results. Notable among these are the distance between the sensor and the surface being scanned, the angle of incidence, the brightness of the projector and ambient light, and the material and color of the object's surface. To quantify these influences, the optimal viewpoint selection algorithm in this study primarily focuses on the distance between the sensor and the surface and the angle of incidence. However, factors such as projector brightness, ambient light brightness, object surface material and color, and the aperture size of the industrial camera lens also significantly affect the quality of the 3D point cloud data collected.

Typically, the darker the object's surface, the lower its reflectivity, resulting in less light information returning to the camera. This degrades the scanning quality, leading to missing point cloud data and reduced accuracy. In overly bright ambient light, data noise increases, and point cloud density decreases, necessitating an increase in projector brightness to enhance the signal-to-noise ratio and ensure scanning quality (this factor notably affects white light structured light scanners; blue light scanners, using different wavelengths, can effectively avoid such interference). For reflective surfaces, increasing projector brightness can cause overexposure or glare, worsening the scanning quality. Transparent surfaces (e.g. glass) require higher precision in scanner parameters and operator expertise, often necessitating specific scanning angles or the use of matte spray coatings to achieve satisfactory results.

Parametrizing the aforementioned influences requires a more realistic and detailed optical simulation environment. However, the optimal viewpoint selection algorithm in this study simplifies the object's surface into a series of triangular patches and does not consider material properties or environmental light factors in the ray casting simulation. Therefore, this study approximates the simulation environment by adjusting ambient light brightness, projector brightness, and using matte spray coatings, which is simpler to implement.

The following Figure 4-5 shows the effect of ray casting in the simulation environment from a zenith viewpoint (zenith angle = 0, azimuth angle = 0) after visibility, occlusion, and optical constraints have been applied. The red areas indicate surfaces that can be scanned.

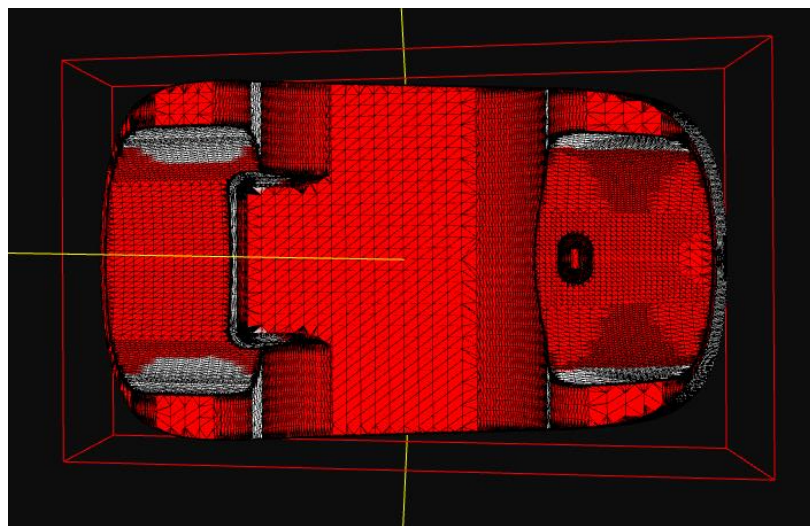
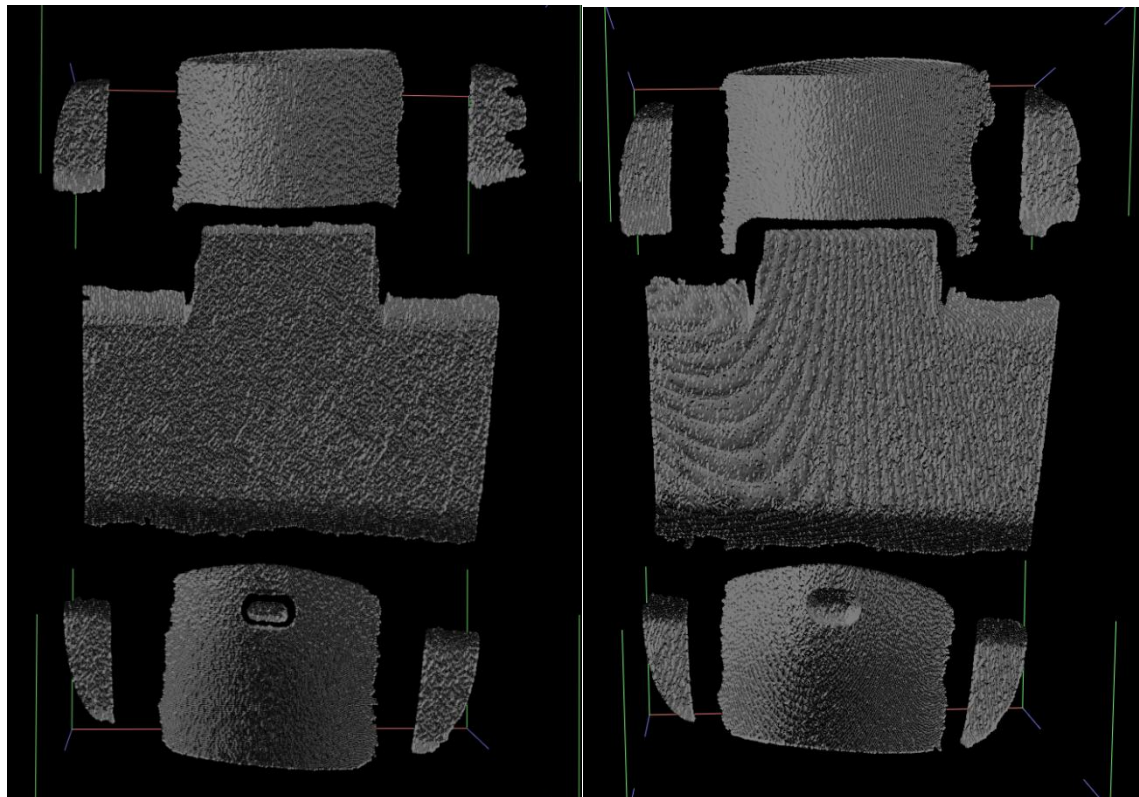


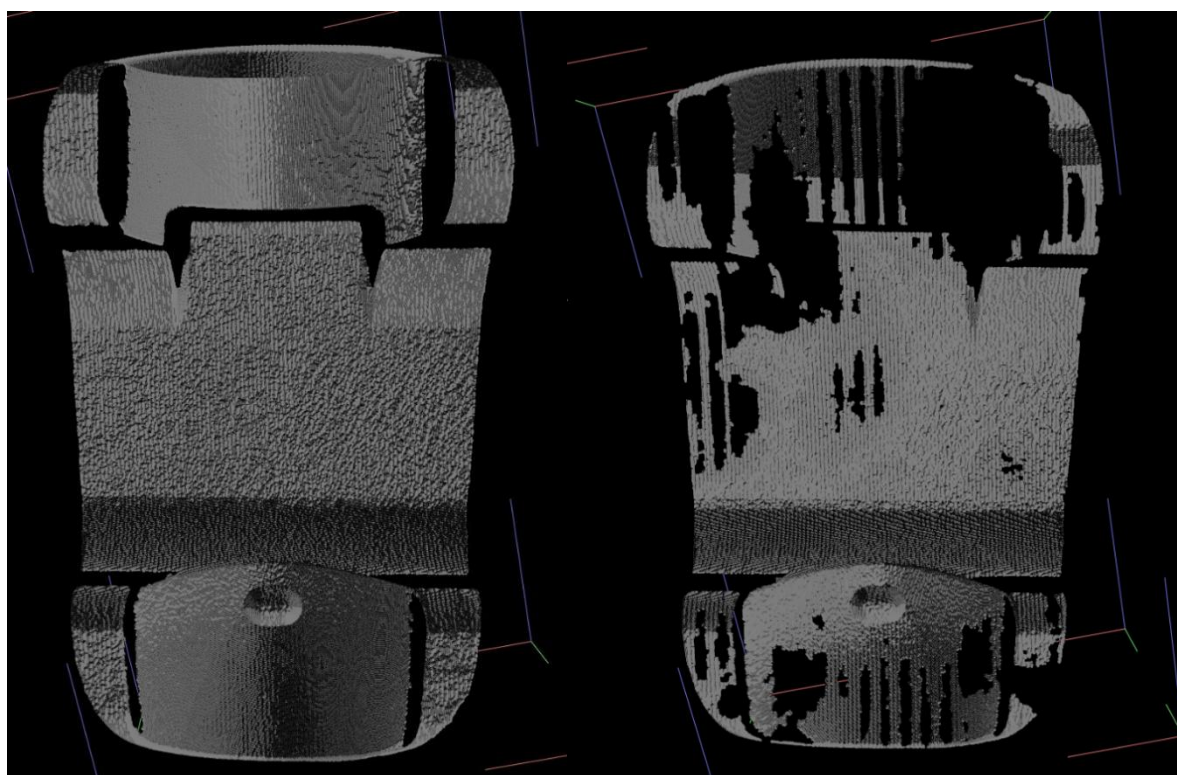
Figure 4-5: Ray casting result in simulation environment from zenith viewpoint

To test the correspondence between the actual scanning lighting effects and the simulated environment, I conducted a controlled experiment. Using the control variable method, I kept the scanner's position and angle, the camera's optical parameters, and the external environmental lighting conditions constant while only adjusting the projector's light intensity. The TranscanC's projector has 10 brightness levels, with 0 being the weakest and 9 being the strongest. The following images show the scanning results with the projector brightness set at levels 1, 3, 5, and 7 for comparison.



(a) Brightness 1

(b) Brightness 3



(c) Brightness 5

(d) Brightness 7

Figure 4-6: Point cloud results from zenith viewpoint in the experimental environment under different projector brightness

Comparison and validation indicate that without using matte spray coatings, a projector brightness setting of 5 yields results closest to the simulation. Minor discrepancies on curved surfaces may be due to deformations caused by internal stresses during the curing process of the light-cured 3D printed samples, which affect the ray casting results.

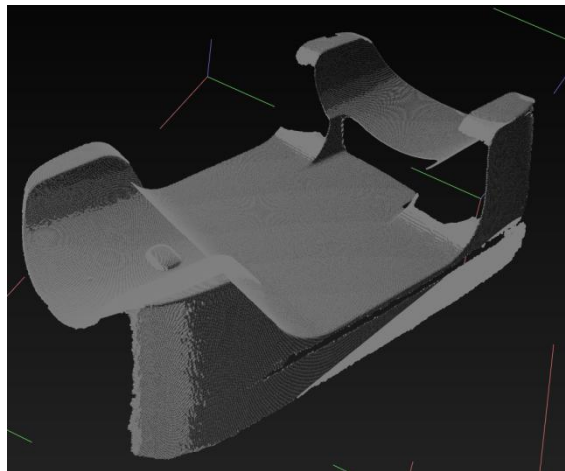
4.2.2 Analysis of Model Scanning Results

To validate the effectiveness of the algorithm, this study first selected the base of an oral scanner as the test sample. This sample features horizontal and vertical planes, concave and convex surfaces, small protrusions, vertical concave angles, and self-occlusion characteristics, making it ideal for testing the validity of the optimal viewpoint selection algorithm due to its moderate size and diverse geometric features.

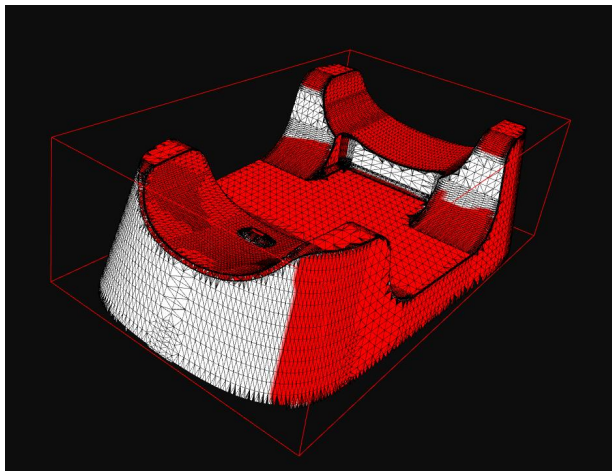
Based on the key algorithm parameters and single-frame point cloud comparison results discussed earlier, the weights for the viewpoint quality evaluation function were set as follows: $a=1$, $b=1$, $e=0.6$, and $f=0.4$. The scanner brightness was set to 5. According to the actual scanning requirements, the stopping criteria for iterative filtering were set to 99% coverage or a coverage growth rate of less than 0.01%. Since the bounding box dimensions of the object are 121*73*37mm, which are smaller than the block unit size of 140*140*140mm, there is no need for block partitioning.

After the iterative filtering of optimal viewpoints, a total of 7 viewpoints were generated, achieving a coverage rate of 98.91%. The viewpoint numbers are 10-31-25-35-11-3-21. When dividing the measurement space into view angles at 45° intervals, viewpoints 10, 11, 3, and 21 belong to the top view, 31 is the right view, 25 is the front view, and 35 is the back view. This indicates that for a flat object like this, top views can capture the most and highest quality information. Based on the standard of the shortest collision-free path for the robotic arm, combined with the rotation of the turntable, the scanning path was planned as a polyline connecting viewpoints 11-10-3-21-35-31-25.

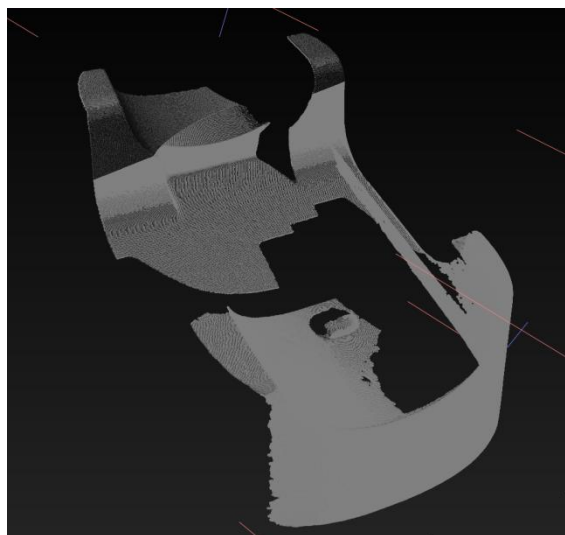
The figure below (Figure 4-7) compares the actual scanning results of each viewpoint with the ray casting simulation results, showing that the simulation results and actual scanning effects are largely consistent. However, due to factors such as surface quality, light reflection intensity, and shape errors of the sample during actual scanning, the obtained point cloud areas may have some defects. Nonetheless, since the frames of the scanning images overlap, the final overall scan file does not exhibit significant defects.



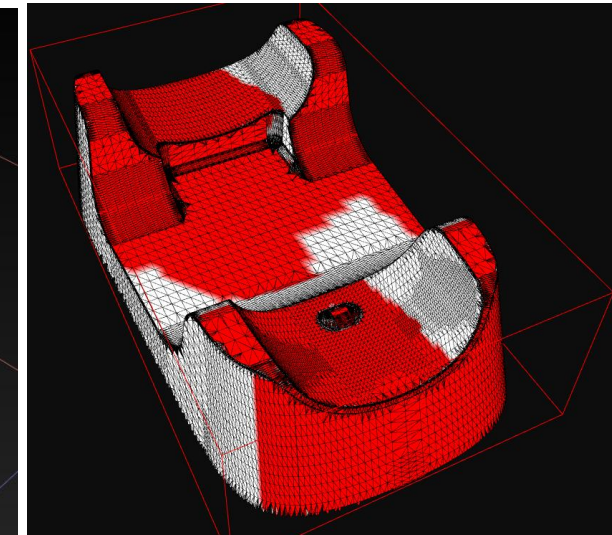
(a) scanning result of Viewpoint 10



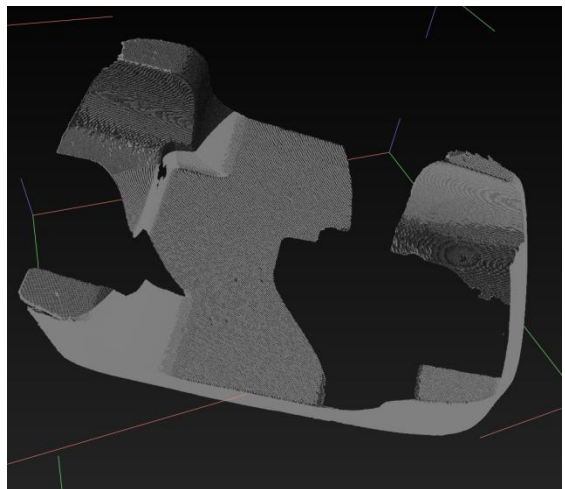
(b) simulation result of Viewpoint 10



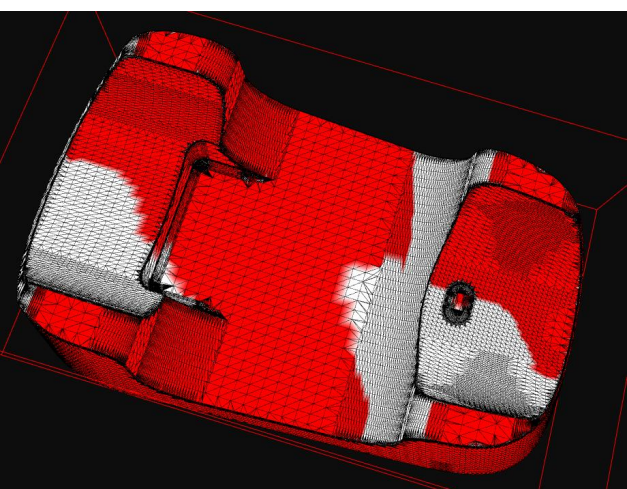
(c) scanning result of Viewpoint 35



(d) simulation result of Viewpoint 35



(e) scanning result of Viewpoint 31



(f) simulation result of Viewpoint 31

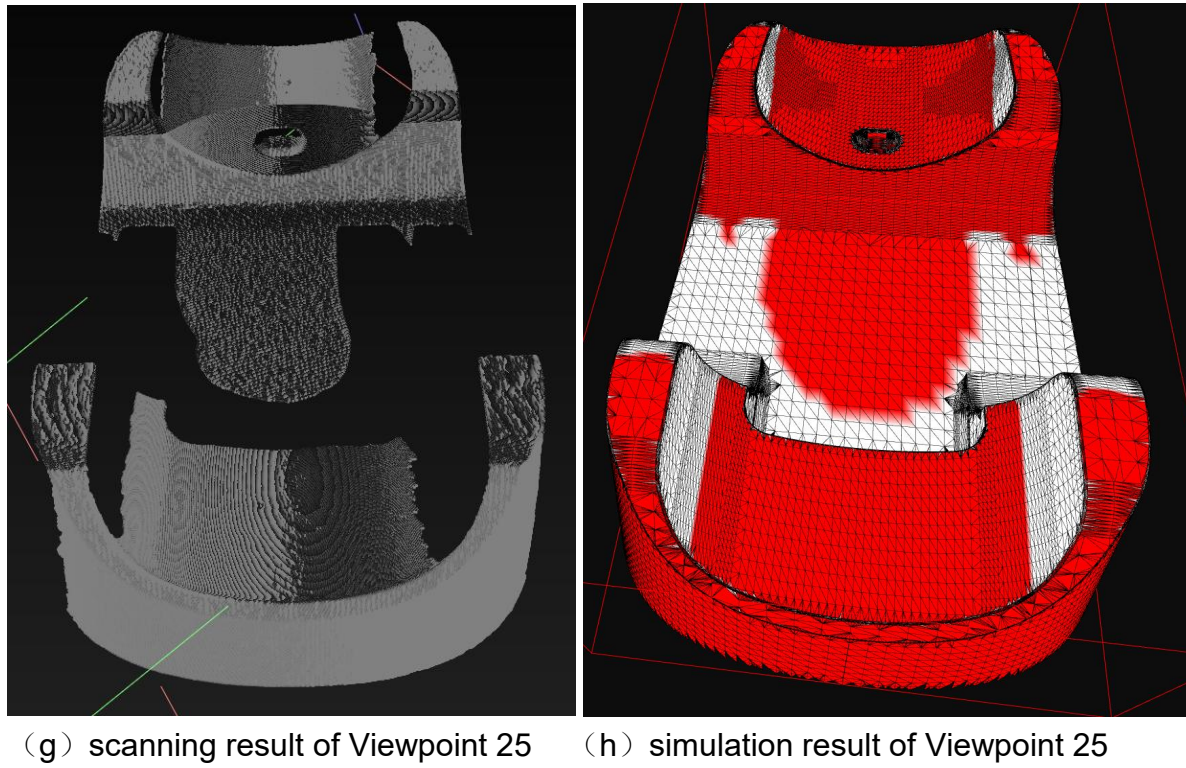


Figure 4-7: The comparison tof actual scanning point cloud and the ray casting simulation results

The following figure (Figure 4-8) shows the actual scanned point cloud file. Analyzing the point cloud data obtained from the actual scan reveals that the model was scanned completely with no significant omissions. When the point cloud file is processed into a triangular mesh and compared with the CAD model, the actual coverage rate of the model is found to be 97%. The missing parts are mainly concentrated in the right-angle concave sections where the horizontal and vertical planes intersect. These areas are small and recessed, and due to the binocular 3D scanner's requirement for both cameras to simultaneously receive grating information to generate point clouds, the imaging quality in these regions is understandably poor. In terms of measurement accuracy, the average measurement deviation for the model's dimensions (length, width, height) is 0.05mm.

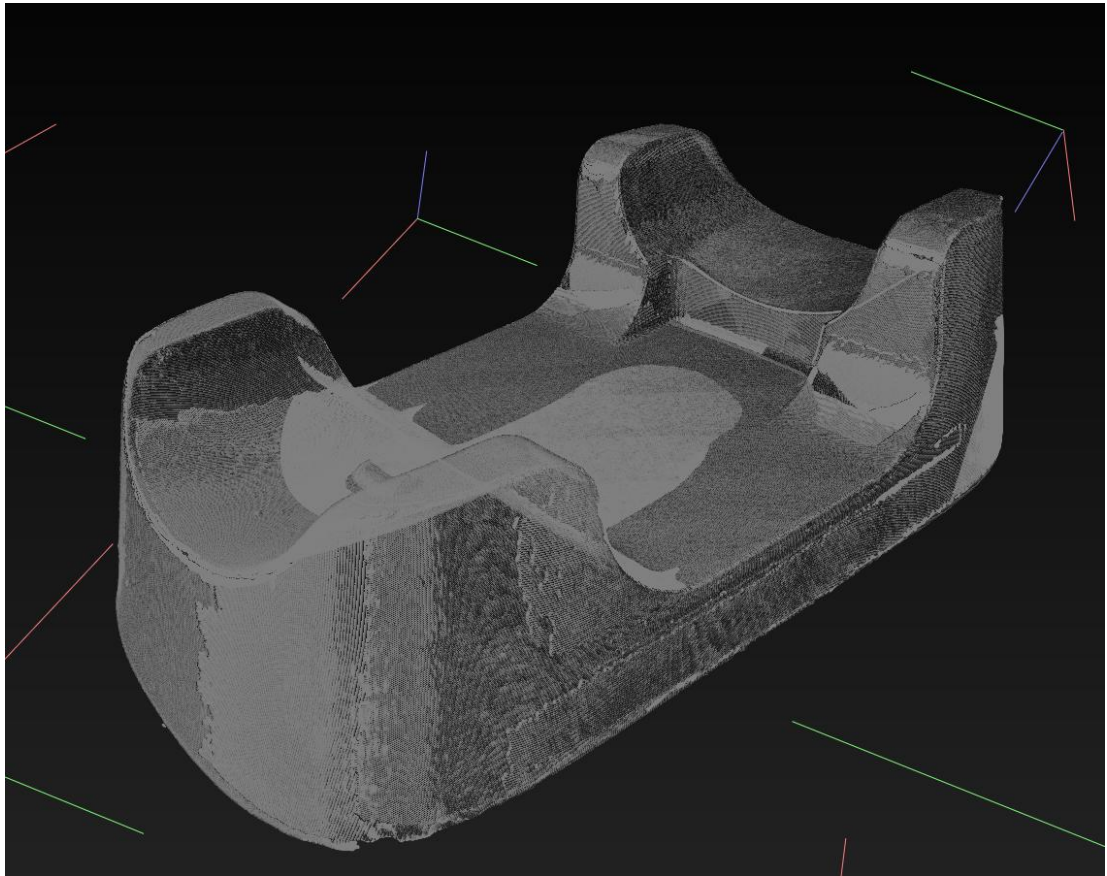
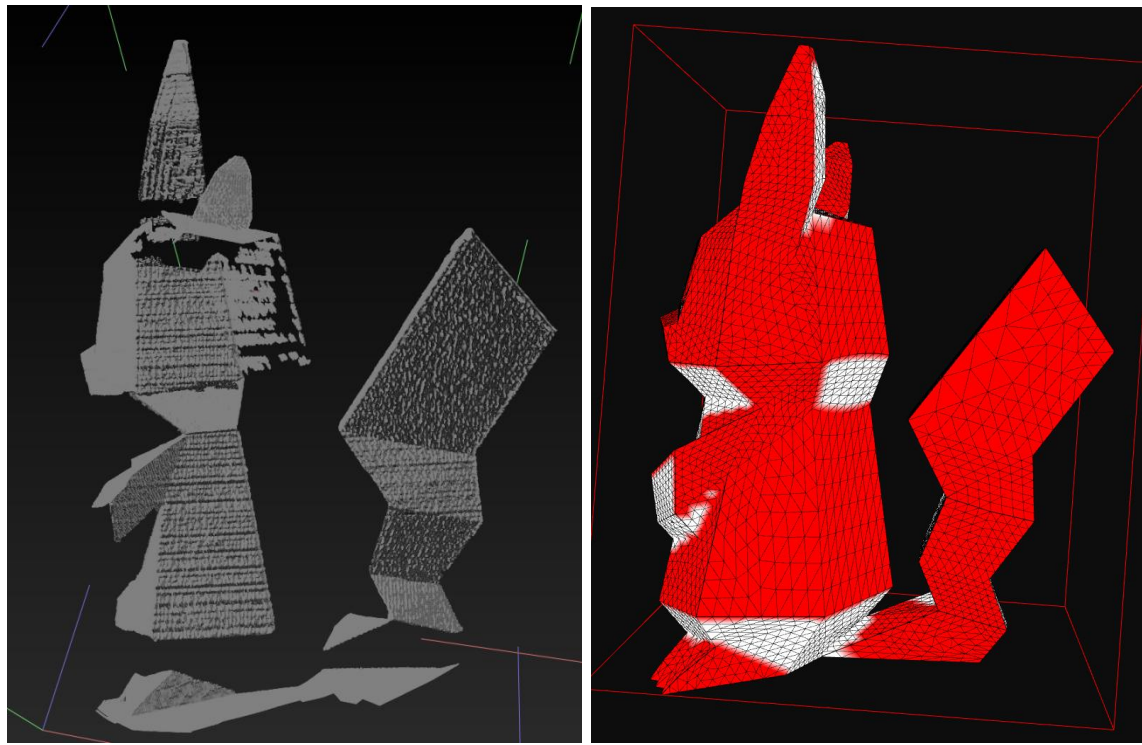


Figure 4-7: The point cloud result of the test sample

Additionally, a medium-sized object was selected for scanning tests to verify the robustness of the algorithm. This Pikachu model also features concave surfaces, numerous inclined planes, and self-occlusion characteristics, making it suitable for testing the optimal viewpoint selection algorithm. Through simulation and iterative filtering, a total of 8 viewpoints were generated, achieving a coverage rate of 99.18%. Given Pikachu's vertical rectangular shape, the viewpoints are more evenly distributed, with one belonging to the top view, one to the left view, and two each for the right, front, and back views.



(a) scanning result of Viewpoint 13 (b) simulation result of Viewpoint 13

Figure 4-8: The comparison of actual scanning point cloud and the ray casting simulation results

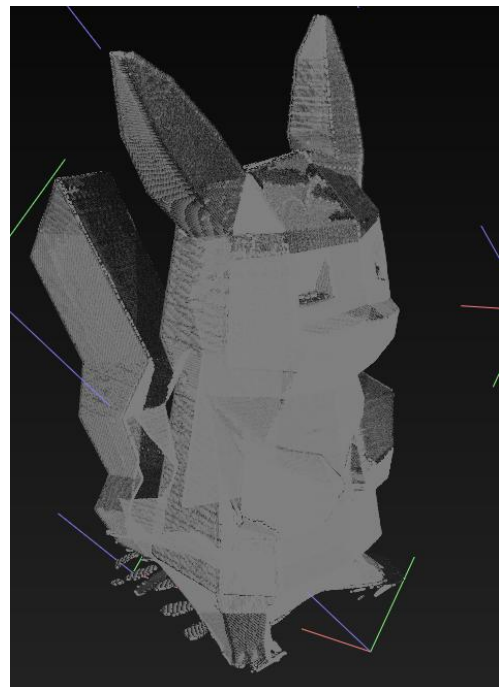


Figure 4-9: The point cloud result of the test sample

Figures 4-8 and 4-9 show the scanning results of the Pikachu model. From the single-frame scanning results in Figure 4-8, it can be seen that there are some discrepancies between the actual scanning results and the ray casting simulation. The possible reasons include the rough surface of the Fused Deposition Modeling (FDM) printed model, which has many small pits affecting light reflection, and slight positioning errors of the object in the actual setup compared to the simulation environment, leading to deviations in scanning angles. From the point cloud of the final scanning results in Figure 4-9, it can be observed that although the model is almost fully scanned, there are differences in point cloud density across various parts. This may be due to certain areas being scanned repeatedly, resulting in overlapping point clouds.

5 Summary and Outlook

5.1 Summary

Structured light 3D measurement technology, with its advantages of being non-contact, high precision, and fast, has found wide applications across various industries. As automation technology advances and application demands increase, 3D reconstruction and inspection are also moving towards automation. Quickly obtaining complete 3D models and applying them to quality inspection has become a key research focus in recent years. Therefore, this thesis primarily focuses on the key technologies of viewpoint planning in 3D measurement.

The main contents of the thesis are as follows:

- **Theoretical Foundations:** This includes the principles of phase-assisted 3D reconstruction, such as camera models, camera calibration, scanning system calibration, and the principles of binocular stereo vision 3D reconstruction.
- **Imaging Range Constraints:** Detailed research was conducted on several constraints affecting the imaging range of 3D sensors during the scanning process. By establishing mathematical models, the measurement space of the system is estimated, and a robust method for generating candidate viewpoint sets based on the measurement space of the 3D scanner and the spatial dimensions of the object is proposed.
- **Imaging Quality Constraints:** Detailed research on constraints affecting the imaging quality of 3D sensors during data acquisition was performed. A simulation environment that effectively mimics the effects of ray casting is established. Based on this, an optimal viewpoint selection function balancing scanning efficiency and quality is developed, along with an iterative algorithm for filtering optimal viewpoints. Experiments demonstrate the accuracy and superiority of this method.
- **Automated 3D Measurement System:** To achieve automation in 3D measurement, an automated 3D measurement system based on a robotic arm, a rotary table, and a structured light 3D scanner is constructed. Using the proposed viewpoint planning algorithm, the optimal viewpoint positions and sight directions for scanning the object are determined. The viewpoint information is converted into commands acceptable to the robotic arm and rotary table based on the transformation matrix obtained from system calibration. Through the controlled movements of the robotic arm and rotary table, multi-viewpoint, fully automated 3D data acquisition and measurement are realized with a single 3D sensor.

- **Experimental Validation:** Experiments show that this method can quickly and conveniently determine the positions and sight directions of viewpoints, providing guidance for one-time measurement of entire objects or automated measurement. This reduces reliance on the engineer's experience and the time required for repeated adjustments, significantly enhancing work efficiency and scanning quality.

In the current research landscape, common viewpoint planning and path planning methods tend to focus solely on surface coverage and scanning efficiency. However, in the practical application of 3D inspection, it is imperative not only to consider the coverage of data but also to ensure the high-precision alignment of scanning data with reference data. This process involves meticulous comparative inspection of both global and local geometric features. The quality of scanning data directly affects the accuracy of geometric construction, which is influenced by a variety of factors, including the distance between the scanner and the object, the normal angle of the object's surface, as well as differences in brightness and surface material. Precise quantitative analysis of these parameters that affect scanning quality is crucial for enhancing the effectiveness of viewpoint and path planning.

Although existing studies have made certain progress in simulation calculations, most have not delved into the translation of simulation results into real-world scanning data. This paper fills this gap by comparing simulated calculations with real-world scanning data, verifying the validity of virtual scanning data, and revealing the differences between it and actual scanning data. This discovery not only confirms the potential of simulation in predicting real scanning effects but also provides valuable insights on how to utilize 3D scanners to obtain higher quality data in real-world applications.

5.2 Limitations and Future Work

This thesis focuses on the technology of viewpoint planning in 3D measurement and has achieved some preliminary experimental results, but there are still several issues that need further research:

- **Slow Computation Speed:** The current computation speed is still slow, and the 3D model of the object contains redundant information, reducing efficiency. Future work will use down-sampling methods to improve efficiency, such as voxelizing the object or redistributing surface patches based on specific rules.
- **Single-Threaded Computation:** Currently, computations are performed using a single-threaded CPU. For large-scale parallel computations like ray casting simulations, GPUs are more suitable. Future work will attempt to use GPUs for ray casting simulations.

- **Insufficient System Calibration:** The current system calibration is inadequate for high-precision scanning experiments. Therefore, improvements in hand-eye calibration are needed to enhance the precision and repeatability of the experimental environment.
- **Insufficient Complexity of Test Samples:** Future tests will involve more complex and larger objects to validate the algorithm's robustness.
- **Modeling Environmental Variables:** Future work will involve mathematical modeling of more variables such as ambient light intensity, projector brightness, and object surface material to study their impact on 3D scanning and reconstruction quality.
- **Diverse Scanner Poses:** The current viewpoints only consider the scanner's horizontal axis pose. Future work will explore more scanner poses to cover a wider range of scanning possibilities, adapting to more diverse application environments.
- **Optimization for Deep and Concave Features:** Due to the structural design and algorithm logic of binocular 3D scanners, many deep and concave features are not effectively covered. Future work will focus on optimizing for special features like deep holes.
- **Improvement of Ray Casting Algorithm:** The current ray casting algorithm uses down-sampling to finite problem space, leading to suboptimal results in areas with sharp edges, high curvature, or densely packed triangular patches. Specialized edge recognition algorithms will be incorporated to improve efficiency and accuracy.
- **Incorporating Reinforcement Learning:** Future work will attempt to incorporate reinforcement learning, using information gain to iteratively generate optimal viewpoints.

Through these improvements and optimizations, we aim to further enhance the performance of 3D measurement systems, meeting the needs of more complex application scenarios.

Bibliography

- [1] Song Zhang, High-speed 3D shape measurement with structured light methods: A review, *Optics and Lasers in Engineering*, 106, 2018, 119-131
- [2] Peuzin-Jubert M, Polette A, Nozais D, et al. Survey on the view planning problem for reverse engineering and automated control applications[J]. *Computer-Aided Design*, 2021, 141: 103094.
- [3] Scott, W., Roth, G., Rivest, J., 2001a. View planning as a set covering problem. NRC Publications Archive doi:10.4224/8913444.
- [4] Karp, R., 1972. Reducibility among combinatorial problems, in: Complexity of computer computations. Springer, pp. 85–103.
- [5] Loriot, B., 2009. Automation of Acquisition and Post-processing for 3D Digitalisation. Phd thesis. Université de Bourgogne.
- [6] Scott, W., Roth, G., Rivest, J., 2001b. View planning for multi-stage object reconstruction.
- [7] Mahmud, M., Joannic, D., Roy, M., Isheil, A., Fontaine, J., 2011. 3D part inspection path planning of a laser scanner with control on the uncertainty. *Computer-Aided Design* 43, 345 – 355.
- [8] Jing W. Coverage planning for robotic vision applications in complex 3d environment[D]. Carnegie Mellon University, 2017.
- [9] Scott, W., 2002. Performance-oriented view planning for automated object reconstruction. Phd thesis. University of Ottawa.
- [10] Martins, F., Gómez García-Bermejo, J., Zalama Casanova, E., Perán González, J., 2005. Automated 3D surface scanning based on CAD model. *Mechatronics* 15, 837 – 857.
- [11] Scott, W., 2009. Model-based view planning. *Machine Vision and Applications* 20, 47–69.

- [12] Loriot, B., 2009. Automation of Acquisition and Post-processing for 3D Digitalisation. Phd thesis. Université de Bourgogne.
- [13] Jing, W., Polden, J., Lin, W., Shimada, K., 2016. Sampling-based view planning for 3D visual coverage task with unmanned aerial vehicle. 2016 IEEE/RSJ International Conference on Intelligent Robots and Systems (IROS) , 1808–1815
- [14] Wei, J., Shimada, K., 2018. Model-based view planning for building inspection and surveillance using voxel dilation, medial objects, and random-key genetic algorithm. Journal of Computational Design and Engineering 5, 337 – 347.
- [15] Jing, W., Goh, C.F., Rajaraman, M., Gao, F., Park, S., Liu, Y., Shimada, K., 2018. A computational framework for automatic online path generation of robotic inspection tasks via coverage planning and reinforcement learning.
- [16] Mohammadikaji, M., Bergmann, S., Irgenfried, S., Beyerer, J., Dachsbacher, C., Worn, H., 2018. Inspection planning for optimized coverage of geometrically complex surfaces, in: 2018 Workshop on Metrology for Industry 4.0 and IoT, pp. 52–67.
- [17] Krause, A., Guestrin, C., Gupta, A., Kleinberg, J., 2011. Robust sensor placements at informative and communication-efficient locations. ACM Transactions on Sensor Networks (TOSN) 7, 31.
- [18] Hepp, B., Nießner, M., Hilliges, O., 2017. Plan3D: Viewpoint and trajectory optimization for aerial multi-view stereo reconstruction. CoRR abs/1705.09314.
- [18] REN Ming-yang, WANG Li-zhong, ZHAO Jian-bo, TANG Zheng-zong. Viewpoint planning of surface structured light scanning for complex surface parts[J]. Chinese Optics, 2023, 16(1): 113-126. doi: 10.37188/CO.2022-0026
- [19] Zhang H, Eastwood J, Isa M, et al. Optimisation of camera positions for optical coordinate measurement based on visible point analysis[J]. Precision Engineering, 2021, 67: 178-188.

- [20] Fan X, Zhang L, Brown B, et al. Automated view and path planning for scalable multi-object 3D scanning[J]. ACM Transactions on Graphics (TOG), 2016, 35(6): 1-13.
- [21] Möller T, Trumbore B. Fast, minimum storage ray/triangle intersection[M]//ACM SIGGRAPH 2005 Courses. 2005: 7-es.
- [22] Prieto, F., 2000. Métrologie assistée par ordinateur. Apport des capteurs 3D sans contact. Phd thesis. Ecole de technologie supérieure.
- [23] Prieto F, Lepage R, Boulanger P, et al. A CAD-based 3D data acquisition strategy for inspection[J]. Machine Vision and Applications, 2003, 15: 76-91.
- [24] Zhang Z. Camera calibration with one-dimensional objects[J]. IEEE transactions on pattern analysis and machine intelligence, 2004, 26(7): 892-899.

Declaration of Compliance

I hereby declare to have written this work independently and to have respected in its preparation the relevant provisions, in particular those corresponding to the copyright protection of external materials. Whenever external materials (such as images, drawings, text passages) are used in this work, I declare that these materials are referenced accordingly (e.g. quote, source) and, whenever necessary, consent from the author to use such materials in my work has been obtained.

Signature:

Stuttgart, on the